MOTION AND STRUCTURE OF THE MAGNETOPAUSE

Michel P. Aubry*, Margaret G. Kivelson

and Christopher T. Russell

University of California, Los Angeles

Institute of Geophysics and Planetary Physics
University of California
Los Angeles, California 90024

Publication No. 865

EXCHANGE DOCUMENT
26 27 28
4
31 ESR

FACILITY FORM 602
N71-20853
(ACCESSION NUMBER)
(THRU)
70
(PAGES)
63
(CODE)
CR-117471
(NASA CR OR TMX OR AD NUMBER)
13
(CATEGORY)

*ESRO-NASA University Research Associate on leave from
Groupe de Recherches Ionospheriques du CNRS (Paris)

Reproduced by
NATIONAL TECHNICAL
INFORMATION SERVICE
Springfield, Va. 22151

INTRODUCTION

The observation of the motion and structure of the magnetopause has been the topic of many papers in recent years (Holzer, et. al., 1966, Heppner, et. al., 1967, Sonnerup and Cahill, 1967, Hyde, 1967, Sonnerup and Cahill, 1968, Cummings and Coleman, 1968, Kaufmann and Konradi, 1968). The importance of this topic lies in the fact that a clear understanding of the magnetopause would enable one to estimate the validity of the so-called open or closed model of the magnetosphere (Dungey, 1961, Beard, 1964), to check the various theories relating to the instabilities of the boundary (Sen, 1965, Parker, 1967 a and b, Lerche, 1967, Southwood, 1968, Alpers, 1969, Karlson, 1970) and to understand the origin of the drag at the magnetosphere boundary. This drag or transfer of momentum through the boundary is evidenced by the existence of the magnetotail and by the direction of the plasma flow at the boundary (Freeman, et. al., 1968, Warren and Freeman, 1970) but there is no present agreement as to the exact physical mechanism involved in the drag (Piddington, 1960, Dungey, 1961, Axford, 1964, Siscoe, 1966, Tsuda, 1967, Eviatar and Wolf, 1968, Coleman, 1970, Cassen and Szabo, 1970). In this paper we present some observations of the boundary motion and structure at times of large drag and indicate the relevance of our observation to the problems described.

It was reported in a previous paper (Aubry, Russell and Kivelson, 1970, hereafter referred to as ARK) that on March 27, 1968 the inbound OGO-5 satellite recorded an inward motion of the magnetopause of about 2 Re in two hours. In this sequence of events, a reversal of the vertical component of the interplanetary magnetic field was immediately followed by an inward motion of the magnetopause caused by an erosion of the magnetosphere; magnetic flux was carried into the tail and the growth phase of a substorm began about half an hour later. The velocity of the inbound OGO-5 satellite roughly matched the average inward velocity of the boundary during about two hours, which enabled us to study the motion and structure of this boundary for a relatively long period of time. Moreover, OGO-5 was transmitting at its highest data rate throughout this period, providing 56 vector samples of the field per second (sps), which allowed us to analyse the fine structure of the boundary.

In section 2, information about the experiment will be provided; in section 3 some basic points of theory will be recalled; section 4 and 5 are respectively devoted to the oscillations and structure of the boundary.

It will be concluded that our observations do not fit any <u>steady</u> open or closed model of the magnetosphere, that the motion of the boundary is at least not inconsistent with the Kelvin Helmholtz instability hypothesis, and that the existence of an observed variable magnetic field component normal to the boundary

could account for the drag responsible for the erosion of the dayside magnetosphere.

2. THE EXPERIMENT

2.1 The Orbit

Some general comments about the OGO-5 orbit were already included in a previous paper (ARK). For convenience, Fig. 1 showing the projection of the OGO-5 orbit in the GSM equatorial plane at the time of our observation is reproduced from this paper. Between 1700 and 1916 UT the distance between OGO-5 and this GSM equatorial plane varied from 1.7 to 0.04 Re and so our measurements were performed essentially in this equatorial plane.

2.2 The Magnetic Field Measurements

The UCLA fluxgate magnetometer was designed to provide an accurate triaxial vector measurement of the magnetic field from perigee at low altitudes to apogee in the interplanetary medium. Each of the three orthogonal sensors has a dynamic range of $\pm 64{,}000$ gammas and in low fields can resolve field changes of 1/8th of a gamma. This was accomplished with a basic magnetometer that measures ± 16 gammas and a set of coils that provide fields to null out the field at the basic magnetometer to within $\pm 16\gamma$. The currents for these coils are provided in 64 steps of 16γ and 128 steps of 1024γ. This is accomplished as follows: If a field of greater than $+16\gamma$ or less than -16γ reaches the basic magnetometer, this field is reduced in steps of 16γ until the field at the basic magnetometer is within its

operating range. When all available 16γ steps have been applied (64 possible) a field of 1024γ is applied and 63 of the 16γ steps are removed. This stepping procedure has a cycle rate of 500 hz which is far above the magnetometer sampling rates.

The measured field consists then of three quantities: the number of 1024γ nulling fields applied, the number of 16γ nulling fields and the output of the basic magnetometer from +16 to -16γ digitized in 256 parts, each 1/8γ. The sum of these three quantities for each independent axis gives the measured vector field.

The basic magnetometer is operated as a closed loop magnetometer with a frequency response that is flat to 150 hz and then rolls off at 20 db per decade above 150 hz. The three possible OGO-5 telemetry rates, 1, 8 and 64 kilobits per second, correspond to Nyquist frequencies of .43, 3.5 and 27.8 hz for the instrument. Since meaningful wave studies can be performed only if no signals above the Nyquist frequency reach the telemetry system, the output of the basic magnetometer enters a bit rate dependent filter before being digitally sampled. This critically damped fourth order filter has 8 db attenuation at half the Nyquist frequency, 20 db attenuation at the Nyquist frequency and 40 db attenuation at twice the Nyquist frequency.

The satellite can simultaneously transmit data to earth (real time data) and store data on the spacecraft on magnetic tape for later transmission (playback data). These data can be sampled at different rates: playback data is always sampled

at 1 kilobit per second whereas the real time data has three possible rates. Thus, the instrument has actually two outputs, each with its independent filter depending on the sampling rate of the digitization unit to which the signal is routed.

The absolute accuracy of the measured field depends on many factors: the sensitivity of the magnetometer, the size of spacecraft fields and the possibility of drifts in the zero levels of the magnetometer. This magnetometer is the most sensitive fluxgate magnetometer ever flown on a spacecraft and is separated from the main body of the spacecraft by a twenty foot boom. However, there are other nearby experiments and this was a newly designed magnetometer. Comparing with the Goddard magnetometers on board which are on a similar boom restricted only to magnetometers, it was found that there was a slow drift from orbit to orbit of the apparent zero levels of the UCLA magnetometer. The Goddard magnetometers consist of a Rb vapor magnetometer and a fluxgate magnetometer both of which have been flown before on OGO-1 and OGO-3 and which provide consistent fields when compared. Data from these magnetometers, graciously supplied by the experimenters have been used to determine the zero level for each OGO-5 orbit. However, in view of the slow drift of the zero levels the absolute value of any one component may be in error from one to two gammas. On the other hand the rate of drift is exceedingly slow compared to the time scales of physical

processes such as waves, discontinuities, etc. Thus changes in the field components can be accurately measured to the digitization window of the experiment, 1/8 gamma.

2.3 Particle Flux Measurements

The pitch angle electron spectrometer was designed to measure the differential unidirectional flux of electrons in the energy range from 45 to 1200 kev. It consists of six approximately coplanar independent detectors, a pair aligned back to back and the other four spaced out through 90° relative to the back to back detectors. The detectors, each of which contains a plastic scintillator and a photomultiplier tube, make simultaneous measurements of electron flux in a cone of half angle 6°, and are capable of analyzing particle energies in eight logarithmically distributed intervals. The measurements are transmitted to earth (real time data) whenever possible, or alternatively, stored on tape for later transmission (playback data). The maximum usable count rate corresponds to a unidirectional flux of 10^{8} electrons/cm^{2}/sec/ster.

During the period of interest on March 28, 1968, the satellite telemetry rate was 64 kilobits per second, at which rate measurements are made in all detectors every .02 sec. The experiment was switched at ten minute intervals from a mode, the energy mode, in which all detectors repeatedly cycled through eight energy channels, to a second mode, the pitch angle mode, in which only total flux, in the energy range was measured.

The total flux in energy mode is obtained by averaging the differential flux over an integral number of cycles. As the averages used in this plot are taken over 70 cycles, the problem of short time variations is not critical. The statistical uncertainty (calculated on the basis of Poisson statistics and the digitization effects resulting from use of a prescaler) is less than 10^3 electrons/cm^2/sec/ster in pitch angle mode and less than three times this in energy mode.

3. MHD DISCONTINUITIES

It is generally agreed that the magnetopause must be mainly a MHD tangential or a rotational discontinuity, the characteristics of which are shown in Fig. 2 (Landau and Lifshitz, 1960). In this figure, ρ, $\underline{v}$ and p are the density, flow velocity and pressure of the plasma; $\underline{H}$ is the magnetic field, and subscripts n and t refer to the components normal and tangential to the boundary. The square brackets [ ] represent the difference between the quantity on the two sides of the discontinuity.

The theory does not define the variation of the field <u>inside</u> the discontinuity. We know only that for a rotational discontinuity, $\underline{H}_1$ and $\underline{H}_2$, the projections in the plane of the boundary of the magnetic field on either side, should be equal in magnitude, a normal component of $\underline{H}$ can exist, and the direction $\underline{H}_1 - \underline{H}_2 = [\underline{H}_t]$ must be parallel to the vector $[\underline{v}_t]$. This last requirement is in fact a very useful test; indeed if we consider the equatorial region of the magnetopause, the plasma flow

velocity on either side must be mainly horizontal and so must the vector $[\underline{v}_t]$. This implies that if the boundary corresponds to a rotational discontinuity the vector $(\underline{H}_1-\underline{H}_2)$ must be mainly horizontal. We shall use these relationships in sections 5 and 6 to identify the nature of the field discontinuity at the magnetopause.

4. MOTION OF THE BOUNDARY

The average inward motion of the boundary between 1700 and 1900 has already been reported (ARK). In that paper it was shown that boundary oscillations superposed on the main inward motion resulted in multiple crossings. We are interested here in studying these oscillations of the boundary in detail.

First, Figs. 3 and 4 present our data. Figure 3, reprinted from ARK, shows the one minute averages of the magnetic field in the geocentric solar magnetospheric (GSM) coordinate system from 1500-2100 UT. The sequence of multiple crossings occurs between 1700 and 1916. The magnetic field and particle data are shown in Fig. 4 which consists of three panels. Each panel refers to the same time interval and contains forty minutes of data. The top line in each panel represents 4.6 second averages of B_1, the component of the magnetic field along the axis 1 of the satellite reference system (in which reference system, the axes are labelled 1, 2, 3). For the period considered, this axis is nearly antiparallel to the Z_{GSM} axis (the angle varies between 170° and 180°) and crossings of the magnetopause appear as reversals of B_1 which is positive in the magnetosheath and

negative in the magnetosphere. In order to avoid any ambiguity, these two regions are labelled in Fig. 4 for the first crossings. The middle line represents 10 sec averages of the particle fluxes for electrons with energy greater than 50 keV. These fluxes were computed from the readings of detector 5 which was oriented at the largest pitch angle. Flux greater than 4×10^4 particles/cm^2/sec/ster is indicated by a straight line, while gaps in the curve occur where data is not available. The bottom line of each panel represents the total magnetic field amplitude.

The first clear encounter of the boundary took place at 1700 UT (Fig. 3) when the geocentric distance of the satellite was 12.8 Re, (point A in Fig. 1). The field amplitude was about the same on both sides of the boundary; only the horizontal component varied. While no particles were detected before 1700, a detectable flux of energetic electrons appeared at 1700, and was observed till 1731 (see Fig. 4). This verifies that the satellite entered the magnetosphere at this time. This fact is confirmed also by the JPL solar wind experiment and the Lockheed ion mass spectrometer on board OGO-5. At this time the field in the magnetosheath was northward and it appears from Fig. 3 that there was essentially one single crossing. By looking at 4.6 sec average data we checked that the small oscillations just before 1700 in Fig. 3 were in fact three partial crossings. So at this time the boundary was not perfectly steady; small amplitude oscillations of 1 to 3 minute periods were present, but their amplitude was much smaller than that of the oscillations observed after 1730 UT.

At 1730 after the reversal of the field in the magnetosheath (as already discussed in ARK), the sequence of multiple crossings began (Figs. 3 and 4). In order to interpret these crossings, we will refer to two models of boundary as sketched in Fig. 5. Model "a" presents a superposition of large amplitude oscillations with periods (T_1) of several minutes, and small amplitude oscillations with periods (T_2) of less than one minute. In model "b" the short and long period oscillations are again superposed but with approximately the same amplitude.

From 1730 to 1840 UT (points B and C in Fig. 4), the occurrences of short duration multiple crossings appear at well spaced intervals and the observations can be interpreted in terms of model "a". The long periods, T_1, range from 3.5 to 6 minutes and the short ones, T_2, can be as short as 10 seconds. For instance, at 1807 a sequence of partial crossings occurs (the one labelled "2" in Fig. 4 will be studied in detail in section 5 and will be shown to correspond to a 10 sec oscillation of the boundary). Between about 1840 and 1903, as discussed in ARK, the magnetosheath field turned more southward; this produced a new inward motion of the boundary and the multiple crossings observed between 1840 and 1906 present a quite different aspect from the former ones. Since now the short duration multiple crossings occur almost continually, they can be explained in terms of model "b" (Fig. 5), with a long period, T_1, of about 5 minutes and a short period, T_2, of about 1 minute or less.

Some minutes after 1900 the magnetosheath field became less southward again and the two last crossings at 1912 and 1915 reflect this situation. Namely the relative amplitude of the short period oscillation has somewhat decreased.

Prior to the reversal of the magnetosheath field at 1730, the peak flux observed by the energetic electron spectrometer is 4×10^4 particles/cm^2/sec/ster. After 1730 the peak flux measured inside the magnetopause increases by an order of magnitude. Oscillations in intensity of the electron flux with periods of several minutes, consistent with the model of large amplitude oscillations of the boundary occur in the regions inside the magnetopause between 1730 and 1844 and after 1905. The period between 1844 and 1905 is characterized by rapid variations in the electron flux, frequently with periods of the order of one minute, and lower peak intensities. Although the oscillations of several minutes period as recorded by the particle experiment are in general agreement with the oscillations of the magnetic field, it can be checked from Fig. 4 that the relative position of the magnetic field and particles boundaries are variable: obviously the picture of a magnetic field boundary dividing two regions with and without energetic particles is too simple.

To be more specific about the motion of the boundary we must describe the motion of the wave forms sketched in Fig. 5. Namely, are they drifting from the front of the magnetopause toward the tail, are they standing, or are they coming from the tail, and what is their velocity? This problem is an important one, because to compute the thickness of the boundary from the time duration of the observed crossings, we must know the velocity of the boundary relative to the satellite. Quite generally, only the velocity normal to the quiet boundary is computed (Holzer, et. al., 1966, Smith and Davis, 1970). However, it appears from theoretical studies that the magnetopause

is often unstable relative to the Kelvin-Helmholtz instability (Sen, 1965, Southwood, 1968) especially when, as in our example, the plasma flow velocity is normal to the magnetic field. It is, therefore, quite probable that the oscillations we observe are a consequence of a Kelvin-Helmholtz instability of the boundary. If this is so, it has been shown by Southwood (1968) that the motion of the boundary is produced by the superposition of two MHD waves propagating parallel to the boundary with opposite phase velocity on either side. If the tailward plasma flow velocity parallel to the boundary is U inside the magnetosphere and U + V just outside the boundary, the motion of the waveforms in Fig. 5 should be tailward with a velocity $U + \frac{V}{2}$.

In the next section we shall show that these multiple crossings can correspond to the tailward drift across the satellite of ripples such as sketched in figure 5 with a velocity of the same order as the plasma flow velocity. This is not inconsistent with the hypothesis that such oscillations are produced by the Kelvin-Helmholtz instability and indicates that the oscillations are not pulsations of the boundary as a whole.

5. STRUCTURE OF THE BOUNDARY

We shall now study some characteristic crossings in our two hour period of observation. For that purpose we shall use the eigenvalue technique discussed in Appendix 1. The magnetic field will be presented in the reference system xyz of the eigenvectors: $\underline{x}$ (largest eigenvalue) is roughly vertical and is

arbitrarily oriented positive upward; z (smallest eigenvalue), normal to the boundary, is generally roughly horizontal and is arbitrarily oriented positive outward. As a consequence, y (intermediate eigenvalue), roughly horizontal too, is positive tailward, and the xy plane is the plane of the boundary.

The directions of the z and x axes corresponding to the smallest and largest eigenvalue for some of the crossings before 1840 are shown in Fig. 6 in the GSM reference system; one second averages were used for computing these eigenvectors. Each point represents the tip of the projection of unitary x (circle) or z (arrow) vectors on the xy GSM plane. Circles corresponding to angles of 30°, 45° and 90° with the GSM Z axis are shown. The arrow labelled z and the circle labelled x correspond to the unperturbed boundary. The cross section of this boundary in the GSM equatorial plane has already been defined in ARK by the relation

$$R = \frac{C}{1 + \varepsilon \cos\alpha}$$

R is the geocentric distance and α the sun-earth-satellite angle (about 40°), $\varepsilon = 0.35$. The satellite is not exactly in the GSM equatorial plane at the time of observation: in order to compute x and z, a magnetopause axisymmetric around the earth-sun line is assumed.

As explained in Appendix 1, there can be a considerable scatter of the eigenvectors computed from different time

intervals even within one particular crossing. We caution the reader not to consider each individual direction in Fig. 6 as meaningful, but to examine the general trend of the pattern. Namely, the $\underline{x}$ directions (circles) make angles generally less than 30° with the GSM Z axis; the $\underline{z}$ directions are extremely variable roughly in the horizontal plane, so the waveforms of Fig. 5 would correspond roughly to an equatorial cross section of the boundary. This corresponds to a fluting of the magnetopause and is in agreement with the results of Kaufman and Konradi (1968).

The sequence of crossings from 1700 to 1916 can be divided into three parts. The first one around 1700 when the magnetosheath field is upward, is characterized by the absence of important fluctuations of the boundary (Fig. 3). The second interesting zone extends between B and C (Fig. 4) and represents a less stable state of the boundary following the partial reversal of the interplanetary field. The crossings numbered 1 to 4 in this zone will be discussed more extensively. The third zone after C (Fig. 4) represents a more unstable state of the boundary following the total reversal of the interplanetary field as already discussed in ARK. The crossings labelled 5 and 6 will be discussed. We shall try to determine whether or not the various states of unstability and the different drags observed in these three parts of the data are associated with a specific structure of the boundary.

5.1 First Zone

In the first zone, the crossing at 1700 has been studied: when examined with the 1 sps data, it consists mainly of a rotation of the field lasting about 15 seconds with no normal component: the computed average for B_z is less than $10^{-2}\gamma$ and so less than the digitization error of the experiment. The crossing was then broken into portions of about 2 sec length and the eigenvalue analysis performed for each of them using the 56 sps data. This analysis confirmed that the boundary had a rather steady orientation during the whole crossing. However, the components of the magnetic field normal to the boundary varied from 10γ to -10γ from one interval to the other. This could be due to the presence of waves inside the boundary.

5.2 Second Zone

Crossing #1

The orientation of the eigenvectors for this boundary are shown in Fig. 6, where for convenience they are labelled $\underline{x_1}$ and $\underline{z_1}$. It appears that the $\underline{z_1}$ axis is very close to the direction of the unperturbed boundary normal.

The variation of the three components of the magnetic field in the reference system of these eigenvectors is shown on Fig. 7 with a sampling rate of 56 sps. The characteristic features of this crossing are: reversal of B_x, maximum of B_y inside the boundary, compressional oscillations of about 4 sec period and 5γ amplitude inside the boundary. The average B_z component, as computed from the one second averaged data, is 2.4γ.

The variation of the tip of the one-second averaged magnetic field in the plane of the boundary as seen from the earth is shown on Fig. 8. This variation is mainly a rotation and the two dashed-line circles centered at C have been drawn for visual convenience. However the ratio $\frac{\underline{H}_1 - \underline{H}_2}{\underline{H}_1}$, which should be zero for a rotational discontinuity, is 0.3 and the direction $\underline{H}_1 - \underline{H}_2$ is mainly vertical (see the direction of x_1 in Fig. 6). These two facts refutes the hypothesis that crossing #1 is a rotational discontinuity. (cf. section 3). In order to check the 2.4γ normal component, the crossing was then broken in intervals of 2 sec length and each of them analyzed by using the 56 sps data. The computed normals to the boundary were rather scattered and the corresponding normal components ranged from +4γ to −23γ. Even if we ignore this last value, there was so much scatter in the normal field that it is probable that the motion of the boundary forbids us from drawing any conclusion from the various normal components obtained and so we do not know if crossing #1 corresponds to a tangential discontinuity. Our main purpose in presenting this crossing was to show an example of a rotating magnetic field across a boundary which is <u>not</u> a rotational discontinuity.

Crossing #2

This is a double crossing; the satellite which is first in the magnetosphere crosses through a bump in the boundary

and makes a short excursion into the magnetosheath lasting several seconds. To study this part of the data, we selected an interval of 21 sec which contains the spike labelled 2 in Fig. 4. Figure 9 shows the variation of the magnetic field in the reference system (1, 2, 3) of the satellite with a sampling rate of 56 sps.

In order to study the magnetic field in a more convenient reference system, an eigenvalue computation from the one-second-averaged data was performed for this interval. This allows us to separate the B_x component which reverses at each crossing from the B_y and B_z components. We assume that $\underline{V}$, the average direction of the field in the $\underline{yz}$ plane is also the direction of the plasma flow which carries the frozen-in field, as well as various bumps on the boundary surface. Each second we plot along $\underline{V}$, starting in a, the direction of the field projection on $\underline{yz}$ (arrows) and the amplitude of the B_x component (Fig. 10). Assuming that at any instant in time the amplitude and orientation of the field are constant along a direction perpendicular to $\underline{V}$, the direction of the flow, we draw the projection of lines of force in the plane yz. The resultant sketch of the boundary explains simultaneously the variation of amplitude and orientation of the field. Between the points a and d the whole picture is self-consistent: namely, given the position of the first crossing at b and the orientation of the field during the following 10 sec, one can predict the position of the second crossing at c; moreover, the values of the B_x component of the magnetic field

around the crossing c can be predicted from their values around the crossing b. This is no longer true beyond the point d (Fig. 10) where a change in orientation and/or amplitude of the plasma flow probably occurs.

For each crossing, b and c, the eigenvector n_b and n_c normal to the boundary were computed from the high time resolution data (56 sps). They are shown in Fig. 10 (bottom left). The orientation obtained for n_b is in agreement with the general shape of the boundary. On the other hand the agreement is not so good for n_c. Owing to the great variability of the boundary at this time we did not try to obtain a better agreement for n_c by selecting several time intervals. The variation of the magnetic field during crossing b, as seen in the reference system of the boundary is shown in Fig. 11. The whole crossing b lasts about one second between M and N. The reference system used is the one corresponding to eigenvectors for crossing b alone. Except for the large difference in time scale (1 sec instead of 10 sec), the pattern is very similar to that observed in crossing #1 (Fig. 7) namely

- reversal of B_x
- maximum of B_y inside the boundary
- fluctuations of B_z around some average value ($\sim -0.5\gamma$)

We think that the usefulness of the method we used for reconstructing the shape of the boundary is confirmed by the coherency of the results obtained. However, we must emphasize its drawbacks: The method would be exact for a rippled <u>tangential</u>

boundary embedded in plasma flow with a velocity uniform in space and constant in the interval of time of the chosen sample, here about 20 sec, and providing the frozen field hypothesis is satisfied. We know that all these conditions are not met; for instance, in the crossing c we obtain a normal component of about 4γ, and around the point d there is some change in the plasma flow. Finally the instantaneous direction of the plasma velocity, assumed to be parallel to $\underline{V}$, at about 30° from the unperturbed boundary for 20 sec, is justified only by the results obtained. Owing to these limitations, Fig. 10 can give only qualitative information about the shape of the boundary but we think that this information is useful. Namely, the very rapid oscillation of the field as exemplified by the spike labelled 2 in Fig. 4 is consistent with the tailward drift across the satellite of small ripples on the boundary.

It is possible to obtain some information about the distances involved in the model of Fig. 10. From the Explorer 35 measurements we know some parameters of the solar wind: temperature: $T_s = 9 \times 10^4\ {}^{\circ}K$, velocity: $V_s = 470$ km/sec, Alfven Mach number = 6.2. From the model of the plasma flow around the magnetosphere for an Alfven Mach number of 8 (Spreiter and Alksne, 1969) the value of these same parameters can be determined for the point of observation (equatorial plane, 0900 LT); we obtain

$$V = 0.4\ V_s = 200 \text{ km/sec}$$

$$T = 19\ T_s = 1.7 \times 10^6\ {}^{\circ}K$$

Let us assume that during 13 sec, between the points a and d of Fig.19, the velocity $\underline{V}$ of the plasma flux was oriented along $\underline{OV}$. This gives us a distance bc, which is half a wavelength of the ripple, of 200 x 9 = 1800 km $\sim$ 0.26 Re. What was the thickness of the boundary at this time? At b the satellite crosses the boundary in 1 sec, at an angle of about 45°. This gives a boundary thickness of 200 x 0.7 = 140 km. Now the Larmor radius for 1.7×10^{6} $^{\circ}$K protons in a 40γ magnetic field is 64 km. So the computed thickness of the boundary at b is about 2 Larmor radii. Theoretically this thickness is a minimum one for a reversal of the field and, consequently, the assumed velocity of the ripple is a minimum one too. This verifies that the ripple responsible for the spike #2 in Fig. 4 has to move tailward with a velocity at least of the same order of magnitude as the plasma flow velocity.

Crossing #3

The position of this crossing in the whole sequence, is shown in Fig. 4. Crossings #3 and #4 have been studied successively and in more detail than the former ones. Indeed they are less than 2 minutes apart which gives an opportunity to study the important changes occurring in the boundary during very short intervals of time. Moreover they seem to be "clean" with the time definition of Fig. 4 and this will allow us to show the importance of high sampling rates for studying the magnetopause. We wanted to check carefully on these crossings

the tailward drift hypothesis as well as the existence of variable components of the field normal to the boundary. This led us to perform several eigenvalue computations for each crossing; this is presented in the Appendix.

In regard to the crossing #3, let us first examine the variation of the magnetic field across the boundary. We have to select some of the time intervals presented in the Appendix: first the interval n_{11} (Fig. A_1) is chosen because it represents one second averaged data for the whole crossing (about 10 sec). In Fig. 12 the variations of $\underline{B}$ in the reference system of the boundary (computed from the n_{11} interval data) is shown. The classical signature of the boundary appears: reversal of B_x, maximum of B_y and oscillations in B_z around an average value (5γ). These features are very similar to those of crossing #1 (Fig. 7) or 2 (Fig. 11). To look in more detail at the region of the field reversal, we choose the time interval N_7 (Fig. A_1) which contains 56 sps data for this region.

In Fig. 13 the variation of the projection of the magnetic field in the plane xy of the boundary (computed from the N_7 interval data) is shown as seen from the earth. This variation should be compared with the rotation in Fig. 8. During the interval AB, the corresponding B_z component varies between -2γ and $+2\gamma$ with an average of 3.5×10^{-2}. If we compute the average B_z component over the whole N_7 interval, the result is somewhat different (-0.5γ as indicated in Table I of the Appendix). This result emphasizes the difficulty of measuring

the component of the field normal to the boundary. It appears that the structure of this part N_7 of the crossing which lasts less than two seconds is rather complicated: a central section NP nearly force-free is squeezed between two intervals MN and PB where opposite Lorentz forces normal to the boundary are maximum ($\underline{B}$ and $\underline{\nabla}B$ are nearly parallel in these two intervals). As a matter of fact, the use of magnetohydrodynamic concepts should be considered here with caution because it will be shown that the total thickness of the boundary during crossing #3 is of the order of 3 Larmor radii.

In regard to the existence of a normal component of the magnetic field to the boundary, it is concluded in the Appendix that no clear result can be drawn for this particular crossing.

Crossing #4

The position of this crossing in the whole sequence is shown in Fig. 4; it occurs less than 2 minutes after crossing #3 and we will use for #4 exactly the same kind of analysis as for #3. A discussion of the eigenvalue analysis is presented in the Appendix. In order to study the variation of the magnetic field across the boundary we first select the interval n_8 which represents one second averaged data for the whole crossing (Fig. A_2). In Fig. 14 the variations of $\underline{B}$ in the reference system of the boundary (computed from the n_8 interval data) is shown. The reversal of B_x and the maximum of B_y are observed. We chose the interval N_6 (56 sps) to look in more detail at the

region of the field reversal. In Fig. 15, the variation of the projection of the magnetic field in the plane of the boundary (computed from the N_6 interval data) is shown as seen from the earth; one observes mainly a rotation. During this interval the corresponding B_z component varies between 11.3γ and 12.6γ with an average of about 12γ. The variation of the field in Fig. 15 is very smooth and we think that the observed normal component of 12γ is not produced by time-dependent fluctuations. It is concluded from the discussion in the Appendix that in crossing #4 there is a component of the magnetic field normal to the boundary; yet this crossing does not correspond to a rotational discontinuity.

Another aim of the study of crossings #3 and #4 was to check the tailward drift hypothesis. For this purpose we consider these two crossings together. It is obvious from Fig. A_1 and A_2 that a change in the orientation of the boundary occurs between the crossings #3 and #4. For crossing #3 the average normal can be assumed to be roughly parallel to the X GSM axis (see the discussion in the Appendix); for crossing #4, the direction of the N_5 arrow is chosen. Fig. 16 summarizes our feeling about the shape of the boundary at the time of crossings #3 and #4, when we neglect the short period oscillations. The angles of 30° indicated in Fig. 16 are not claimed to be meaningful to better than $\pm 10^\circ$. The important point we want to emphasize is that the relative orientation of the two normals associated with the fact that #3 is observed before #4, implies that the structure AMB moves toward the tail.

What are the dimensions involved in this structure? First, we make the assumption that its tailward velocity is the velocity of the plasma flow (200 km/s) parallel to the unperturbed boundary. The distance AB represents 2 minutes, or $120 \times 200/6.4\ 10^3 \sim 3.5$ Re which can be compared with the 0.3 Re obtained in the case of spike #2 (distance bc in Fig. 10). To evaluate the thickness of the boundary we have to correct for the oscillations occurring during the crossing. The technique used is simple: from the slope of the unperturbed part of the crossing we evaluate graphically the duration of this crossing in the absence of oscillation. From Figs. A_1 and A_2 this gives about 2 sec for crossings #3 and #4. The angle between the velocity (200 km/s) and the boundary is $\pm 30^\circ$ for the two crossings; we obtain a thickness of 200 km equivalent to 3 proton Larmor radii. Alternatively, if this boundary thickness is considered to be a reasonable one, our result checks that the order of magnitude assumed for the velocity of the boundary was correct. So for the short or long period oscillations of the boundary (spike #2, or the pattern defined by crossings #3 and #4), we reach identical conclusions: these oscillations are consistent with ripples on the boundary, drifting tailward with a velocity of the same order of magnitude as the plasma flow velocity.

5.3 Third Zone

For the third zone of crossings after 1840, we tried to analyse the spikes labelled 5 and 6 in Fig. 4 by the technique already used for the spike #2 but this attempt was unsuccessful. Although no conclusion can be shown for this third zone we think that it can be useful to present a short account of the difficulties involved. Spike #5 appears very similar to spike #2 even at a resolution of 7 sps. Its duration is about the same, namely 10 to 15 sec, but the eigenvectors computed from the 56 sps data for five different intervals were so scattered, with components normal to the boundary ranging from -15γ to $+20\gamma$, that we were unable to devise a scheme equivalent to that of Fig. 9 for spike #5. For spike #6, the high resolution data (56 sps) presented in Fig. 17 shows that a study using the eigenvalue technique is meaningless: the fluctuations are too much rapid. Figure 17 represents the total field B_T and the three components of the field in the satellite reference system.

Two remarks about this spike can be useful. Till 1846:30, OGO-5 was in the magnetosheath and some seconds later the boundary swept partially over it. The first thing recorded by the satellite just outside the boundary was a very high magnetic field peaking at 70γ during less than 2 sec at about 1846:33; such large amplitude fields were never recorded before 1800. After this time we have two more examples (see 1859 and 1913 in Fig. 4).

Another characteristic of the boundary at this time was the very high level of oscillations with periods less than 1 sec. In this regard, it is interesting to compare Fig. 17 with Figs. 7, 9, A_1 and A_2 which show crossings #1, #2, #3 and #4 with the same sampling rate. The main conclusion to be drawn from these very brief comments about the third zone is that owing to the great variability of the boundary at this time, one cannot assume this boundary to keep even a roughly constant orientation during the time required for one crossing, and so the usual analysis technique fails.

6. DISCUSSION AND CONCLUSION

We now summarize and discuss the main new findings of this study.

Motion of the Boundary. From the observation of crossings we measured periods of several minutes and periods of less than one minute, even as low as 10 seconds. The two ranges do not seem to overlap. This is confirmed by the particle data. The long period oscillations are well within the period range reported by Hyde (1967), Anderson, et. al., (1968), Kaufmann and Konradi (1968), Smith and Davis (1970). They are shorter than those reported by Holzer, et. al., (1966). The Kelvin-Helmholtz instability is generally proposed as an explanation of these oscillations (Southwood, 1968). We have shown on two examples (crossings #3 and #4) that the waveform associated with these oscillations drifted tailward with a velocity of the same

order of magnitude as the plasma flow velocity as would be required for a wave generated by the Kelvin-Helmholtz instability.

The short period oscillations have not yet been reported in the literature, the main reason being that very often the sampling rate of the data did not permit the study of short periods. This was the case for Explorer 12 for instance (Hyde, 1967, Kaufman and Konradi, 1968). In the case of IMP 2 the particle flux measurements were made every 40 sec; the fact that the spectrum of oscillation period obtained from IMP 2 dropped sharply below 3 minutes (Anderson, et. al., 1968) confirm that the two ranges of oscillation namely several minutes and less than one minute are separated. We do not know if this implies two different generation mechanism, but we have shown that the 10 sec period ripple on the boundary responsible for the spike #2 was also drifting tailward with a velocity similar to the plasma flow velocity. It would be interesting to know if the fluctuation of the order of 10 seconds as represented by spikes #2, #5, and #6 have a different origin from the ones with less than 5 sec periods which appear in crossings #1 (Fig. 8), #2 (Fig. 11), #3 (Fig. A_1) #4 (Fig. A_2), and #6 (Fig. 17). Let us recall that the proton cyclotron period in a 30γ magnetic field is about 2 sec. The amplitude of the long period oscillations is generally much larger than the amplitude of the short period ones, except during the last part of the crossing

(between 1840 and 1906). It should be emphasized that this last sequence of crossings is characterized by:

- the most southward orientation of the magnetosheath field
- the most inward position of the boundary
- the most fluctuating magnetic fields and particle fluxes

This is in contrast to the nearly steady boundary recorded at 1700 where the magnetosheath field was northward. The oscillations as recorded by the particle experiment confirmed the qualitative description obtained from the analysis of the magnetic data.

We assumed that the multiple crossings observed at the satellite are produced by the drifting toward the tail, of ripples on the boundary, with a velocity of the same order of magnitude as the average flow velocity of the plasma, (about 200 km/sec). The boundary thickness computed from this model was of 2 to 3 protons Larmor radii; if this thickness is considered to be a reasonable one, this is a rough check of the validity of our assumption on the velocity. The relative orientation of the boundary during succeeding crossings confirms that the motion was indeed tailward (a similar conclusion was reached by Kaufmann and Konradi, 1968).

Microstructure of the Boundary

We analyzed more than twenty crossings, four representative ones have been presented. Various signatures have been found as can be checked from Figs. 7 to 15. Moreover the evolution, as seen by the satellite, from one shape to the other is very

rapid: for example, there is a delay of only two minutes between the structures observed in Figs. 13 and 15. However, a fact remains constant through the whole interval: the difference vector of the magnetic fields on the two sides of the boundary is mainly vertical. The measurements being made at the equator, the difference vector for plasma flow velocity should be mainly horizontal. Therefore, we claim that the results cannot fit with a rotational discontinuity model of the boundary. This is confirmed by the fact that the amplitudes of the field on the two sides of the boundary always differ by at least 20%. On the other hand it has been shown also in section 5 that at some of the observed crossings, normal components of the magnetic field are present and so these crossings cannot be interpreted as tangential discontinuities either.

Normal Component

The existence of a normal component of the magnetic field is probably the most important part of any study of the magnetopause because it is customarily related to the open and closed models of the magnetosphere (Dungey 1961, Beard 1964). From a theoretical point of view, it has been shown by Siscoe (1966) that a uniform normal component over the whole magnetopause should be roughly $10^{-2}\gamma$. Many previous attempts to determine the normal component of the magnetic field experimentally failed to obtain definitive results. One reason, as discussed in the Appendix, is that only high sampling rates permit the study of a highly time dependent magnetopause. However, in our opinion,

the main reason is that such a "definitive result" does not exist. First, our observations show that from one crossing to another very varying average normal components appear. In the four examples presented, these average normal components were mainly positive, but we observed also negative or inward normal components. Secondly, inside each crossing the normal component could fluctuate by several gammas which is far from negligible when compared with a total field occasionally as low as 10γ in the middle of the current sheet. Owing to this variability, we cannot compare our results with the uniform normal component assumed by Siscoe (1966). These various normal components, which were never associated with a structure of rotational discontinuity, are undoubtedly related to the very high drag observed at this time and already reported in ARK.

This study concerns a short interval of time and consequently does not pretend to give any statistical information. However, we had the opportunity to study a very perturbed state of the magnetopause and it is worthwhile to summarize the observations presented in ARK and in this paper. On March 27, 1968, following a reversal of the interplanetary magnetic field from northward to southward, some large amplitude oscillatory motions developed on the magnetosphere boundary; at the same time the very structure of this boundary was very variable and this variability increased with the southward component of the interplanetary field. Associated with these phenomena, variable components of the magnetic field normal to the boundary were recorded and

produced a large transfer of momentum across the magnetopause leading to the erosion of the dayside magnetosphere. It must be emphasized that during all this period of time, the observed local characteristics of the boundary, including the amplitude and orientation of the normal component as well as the counting rate of energetic electrons on either side of the boundary, were extremely variable and thus did not fit with any steady open or closed model of the magnetosphere.

APPENDIX

For the detailed study of individual crossings, the first problem is to display the variations of the magnetic field in a convenient reference system. In particular we wish to choose the $\underline{x}$ and $\underline{y}$ directions to be in the plane of the boundary and $\underline{z}$ normal to the boundary. The technique for determining this reference system is now very well known (Sonnerup and Cahill 1967). Since $\underline{B}$ must satisfy

$$\underline{\nabla} \cdot \underline{B} = 0, \tag{A.1}$$

if we assume a plane homogeneous boundary such that

$$\frac{\partial \underline{B}}{\partial_x} = \frac{\partial \underline{B}}{\partial_y} = 0 \tag{A.2}$$

then

$$\frac{\partial B_z}{\partial_z} = 0 \tag{A.3}$$

If σ^2 is the variance of the projection, on a direction $\underline{n}$, of a sample of N measurements of the magnetic field,

$$\sigma^2 = \frac{1}{N} \sum_{i=1}^{N} \left[\underline{B_i} \cdot \underline{n} - \overline{\underline{B}} \cdot \underline{n} \right]^2, \tag{A.4}$$

then Eq. (A.3) implies that σ^2 should be zero when $\underline{n}$ is parallel to the normal to the boundary, but in practice this will not be entirely true due to the presence of waves and because the boundary is not planar nor homogeneous. The maximum and minimum values of σ^2 are obtained by computing the eigenvalues of the matrix

$$M_{\alpha\beta} = \overline{B_\alpha B_\beta} - \overline{B_\alpha}\,\overline{B_\beta}$$

where B_α and B_β are components of an individual measured field vector in the reference system of the satellite.

The vector associated with the smallest eigenvalue is normal to the boundary. The vectors $\underline{x}$ and $\underline{y}$ associated respectively with the largest and intermediate eigenvalues, are in the plane of the boundary. If the current inside the boundary is unidirectional, $\underline{x}$ is perpendicular to the current vector and then $\underline{y}$ and $\underline{z}$ are undetermined.

Some remarks should be made: the method is based on the validity of Eqs. (A.2) and (A.3) which requires a plane and steady state boundary during the time of the analysis. A crossing as seen by OGO 5 lasts about 10 seconds and we have shown evidence for important variations of the orientation of the boundary within such a time interval. Thus, at least in our application, Eqs. (A.2) and (A.3) are not generally satisfied over an entire crossing. It is, therefore, important in applying the eigenvalue technique to boundary crossings to select for analysis, intervals short enough that the boundary remains relatively steady. In

this appendix we illustrate for two crossings the effect of changing the interval of analysis across a boundary traversal and of changing the sampling rate of the data used in the analysis. For the UCLA OGO-5 fluxgate, changes in sampling rate are equivalent to averaging the data points over different sample periods because the data is filtered to obey the Nyquist criterion at each sampling rate.

First, let us make an eigenvalue analysis for crossing #3. An enlarged plot of the B_1 component for this crossing measured at a rate of 56 sps is shown in Fig. A1. Eigenvalue computations have been processed for eleven time intervals shown on this figure. For the intervals labelled N_1 to N_9, a rate of 56 sps was used; for the intervals labelled n_{10} and n_{11}, 1 sps was used.

Table 1 lists the following information for these eigenvalue computations: the number of samples used to perform the eigenvalue computation, the average component B_z of the magnetic field normal to the boundary as well as the variance σ^2(Eq. (A4))of the normal component of the field around this average value; (this of course equals the smallest eigenvalue). The ratio of the largest eigenvalue to the intermediate one as well as the ratio of the intermediate to the smallest one are also shown for each interval.

Table 1 shows several facts about the eigenvalue analysis. First, the field along the computed normal is quite variable ranging from 10 to -20γ. Secondly, the variance of the field

along the normal can be quite small, as low as $.03\gamma^2$ and is largest for the intervals covering the longest period of time. Thirdly, the three eigenvalues generally have quite distinct magnitudes. We shall return to the first point later. The second point implies that the boundary orientation does not change much over short periods but can move significantly over long periods. The third point means that the direction of maximum field variation (the $\underline{x}$ axis) and of minimum field variation (the boundary normal) are both well defined. However, the 56 sps data generally give a better separation of the intermediate and minimum eigenvalues than does 1 sps data, and thus we expect the 56 sps data defines the boundary normal better.

The directions $\underline{z}$ of the normal to the boundary (arrows), and of the $\underline{x}$ axis (circle) obtained in these eleven computations are shown at the upper left of Fig. A1. The representation is the same as in Fig. 6, namely each point (arrow or circle) represents the projection in the GSM equatorial plane of the tip of a unitary eigenvector. Circles corresponding to angles of 10°, 30° and 90° with the GSM Z axis are shown. The dashed arrows (N_2, N_3, N_4 and N_5) represent vectors below the $\underline{XY}$ GSM plane. Except for these four vectors, all the eigenvectors in Fig. A1 have a positive component along the GSM Z axis.

The variation of the boundary orientation during this crossing can be studied from the evolution of the $\underline{z}$ eigenvectors (arrows). These vectors have been grouped in three sets (shaded areas): N_2 and N_3 correspond to the first 1 second part of the

crossing around 1817:08 UT; N_7, N_8 and N_9 correspond to the last part, 2 seconds around 1817:12; the intermediate part lasting 3 seconds is represented by N_4, N_5 and N_6. The N_1 $\underline{z}$ vector is computed from the whole interval and so represents some time average of the boundary normal direction. However, one must not forget that the time spent by the satellite inside a region of the boundary at a particular time depends on the angle between the instantaneous normal and the velocity vector of this part of the boundary (a velocity vector parallel to the normal gives the shortest crossing, whereas a velocity vector parallel to the boundary gives the largest one). Consequently the time-averaged normal (as the N_1 arrow) can be different from the space-averaged normal we are interested in. For this particular crossing (#3) the latter normal is probably not far from the X_{GSM} axis. The results obtained from the 1 sps data are rather different from the results obtained from the 56 sps data even when the interval is exactly the same (n_{11} and N_1 for instance) and we show them only to illustrate the advantage of the high time resolution data.

The largest eigenvectors (circles) are on the average not very far from the Z GSM axis (see N_1, n_{10} and n_{11}) a result which would be obtained from a current sheet flowing on the average very roughly parallel to the GSM equatorial plane. However, the structure of this current sheet is rather complicated as can be checked from the scattering of the largest eigenvectors obtained from short time samples (N_2 to N_9).

Let us now examine the eigenvalue analysis for the crossing #4. An enlarged plot of the variation of the B_1 component measured at a rate of 56 sps is shown in Fig. A2. Ten intervals chosen for the eigenvalue computation are delineated and the directions of the corresponding axes x and z are shown in the upper right of the figure.

Table 2 presents the information about this set of eigenvalue computations in the same format as used in Table 1. As before the component of the field normal to the boundary varies over the different analysis intervals, ranging from 4.4 to 13.6γ. Again the ratio of the intermediate to the smallest eigenvalue illustrates that the 1 sps data can only poorly define the direction of the boundary normal. Also, as before the longer intervals are associated with larger variances.

Examining Fig. A2, we see that the z eigenvectors are less scattered than those in crossing #3. In fact the main scatter is due to n_8, n_9 and N_2. The calculation of n_8 and n_9 used 1 sps data which, as discussed above, poorly define the normal, and the interval over which N_2 was calculated includes a bump which appears to be due to a short period fluctuation with a period of the order of seconds of the same type which produced an intermediate zone in crossing #3. If these three normals are ignored, the grouping of the calculated normals around some average normal direction is apparent.

The computed x-axes (circles) lie as expected, roughly in a plane perpendicular to this average normal. (The intersection

of this plane with the unit sphere is indicated by the dashed line.) Here, again, the $\underline{x}$-axes corresponding to the long duration samples N_7, n_8, n_9 and n_{10} are closest to the Z GSM axis which is consistent with a current sheet flowing approximately in the GSM equatorial plane. The scatter of the $\underline{x}$-vectors computed over the shorter intervals reflects the complexity of the detailed structure of the current sheet.

From an examination of these two crossings we see first that we generally cannot determine consistent boundary normals with the 1 sps data. Furthermore, even the 56 sps data may give misleading normals at times when the boundary oscillates during an analysis interval. Thus we must use the results of the eigenvalue technique with caution, requiring a consistent pattern of normals over short periods within the boundary if we are to obtain meaningful results. High data rates such as available on OGO-5 are essential for this purpose, although low sampling rates certainly are adequate to give a general picture of the field variation across the boundary (as in Figs. 8, 10, 12 and 14).

With this in mind we can interpret the extent to which the field component normal to the boundary as derived in Tables 1 and 2 is meaningful. First, we should ignore all the components derived from the 1 sps data. In the crossing #3 the various B_z components (Table 1) are very variable and both positive and negative so we cannot claim a steady normal component exists

during this crossing. On the other hand, if we discard the 1 sps data, the normal components obtained for the various time intervals in the crossing #4 (Table 2) are rather constant of the order of 10γ. The only exception is the interval N_2 which is a perturbed part of the crossing. The rather steady normal component during the remainder of the crossing shows that this measured normal component is not a consequence of fluctuations in the orientation of the boundary. As the error in zero-level discussed in section 2 is less than 2γ for each axis, a zero-level error cannot explain such a 10γ normal component either. Thus, we see that at times there can exist large field components normal to the magnetopause.

Acknowledgments

We wish to thank the many experimenters who permitted us to examine their data for the interval covered in this paper: Drs. D. Colburn and C. Sonett of Ames Research Center for the Explorer 35 and Explorer 33 magnetic field data; Marcia Neugebauer of JPL for the OGO-5 solar wind plasma data; Drs. S. Ossakow and G. Sharp of the Lockheed Palo Alto Research Laboratory for the OGO-5 ion mass spectrometer data and Drs. T. Skillman and J. Heppner of GSFC for providing us with data to check our zero levels.

Helpful discussions with P.J. Coleman, Jr., F. Coroniti, T. Farley, R. Holzer, C. Kennel and G. Siscoe are also gratefully acknowledged. The co-investigators responsible for the UCLA fluxgate magnetometer are: P.J. Coleman, Jr., Thomas A. Farley and Darrell L. Judge.

This work was supported by the National Aeronautics and Space Administration under NASA contract NAS5-9098. One of us (M.P.A.) also received support from ESRO and NASA.

Bibliography

Alpers, W., Steady state charge neutral models of the magnetopause, Astrophys. and Space Sci., 5, 425-437, 1969.

Anderson, K.A., J.H. Binsack and D.H. Fairfield, Hydromagnetic disturbances of 3 to 15 minutes period on the magnetopause and their relation to bow shock spike, J. Geophys. Res., 73, 2371-2386, 1968.

Aubry, M.P., C.T. Russell and M.G. Kivelson, On inward motion of the magnetopause preceding a substorm, Pub. No. 846, IGPP, UCLA 1970.

Axford, W.I., Viscous interaction between the solar wind and the earth's magnetosphere, Planet. Space Sci., 12, 45-53, 1964.

Beard, D.B., The effect of an interplanetary magnetic field on the solar wind, J. Geophys. Res., 69, 1159-1168, 1964.

Cassen, P. and J. Szabo, The viscous magnetopause, Planet. Space. Sci., 18, 349-366, 1970.

Coleman, Jr., P.J., Tangential drag on the geomagnetic cavity, to be published in Cosmic Electrodynamics, 1970.

Cummings, W.D. and P.J. Coleman, Jr., Magnetic fields in the magnetopause and vicinity at synchronous altitude, J. Geophys. Res., 73, 5699-5717, 1968.

Dungey, J.W., Interplanetary magnetic field and the auroral zone, Phys. Rev. Letters, 6, 47, 1961.

Eviatar, A. and R.A. Wolf, Transfer processes in the magnetopause, J. Geophys. Res., 73, 5561-5575, 1968.

Freeman, J.W., Jr., C.S. Warren and J.J. Maguire, Plasma flow directions at the magnetopause on January 13-14, 1967, J. Geophys. Res., 73, 5719, 1968.

Heppner, J.P., M. Sugiura, T.L. Skillman, B.G. Ledley and M. Campbell, OGO A magnetic field observations, J. Geophys. Res., 72, 5417, 1967.

Holzer, R.E., M.G. McLeod and E.J. Smith, Preliminary results from the OGO 1 search coil magnetometer: Boundary positions and magnetic noise spectra, J. Geophys. Res., 71, 1481-1486, 1966.

Hyde, R.S., Explorer 12 magnetometer observations of the magnetosphere boundary region, Publication UNH 67-6 of the Department of Physics of the University of New Hampshire, 1967.

Karlson, E.T., On the equilibrum of the magnetopause, J. Geophys. Res., 75, 2438-2448, 1970.

Kaufmann, R.L. and A. Konradi, Explorer 12 magnetopause observations: Large scale non uniform motion, Goddard Space Flight Center, Report X-612-448, 1968.

Landau, L.D. and E.M. Lifshitz, Electrodynamics of continuous media, Pergamon Press, 1960.

Lerche, I., On the boundary layer between a warm, streaming plasma and a confined magnetic field, J. Geophys. Res., 72, 5295-5310, 1967.

Parker, E.N., Confinement of a magnetic field by a beam of ions, J. Geophys. Res., 72, 2315-2322, 1967a.

Parker, E.N., Small-scale non equilibrium of the magnetopause and its consequences, J. Geophys. Res., 72, 4365-4374, 1967b.

Piddington, J.H., A theory of polar geomagnetic storms, Geophys. J. of Royal Astron. Soc., 3, 314, 1960.

Sen, A., Stability of the magnetospheric boundary, Planet. Space Sci., 13, 131-141, 1965.

Siscoe, G.L., A unified treatment of magnetospheric dynamics with application to magnetic storm, Planet. Space Sci., 14, 947-967, 1966.

Smith, E.J. and Leverett Davis, Jr., Magnetic measurements in the earth's magnetosphere and magnetosheath: Mariner 5, J. Geophys. Res., 75, 1233-1245, 1970.

Sonnerup, B.U.O. and L.J. Cahill, Jr., Magnetopause structure and attitude from Explorer 12 observations, J. Geophys. Res., 72, 171, 1967.

Sonnerup, B.U.O. and L.J. Cahill, Jr., Explorer 12 observations of the magnetopause current layer, J. Geophys. Res., 73, 1757-1770, 1968.

Southwood, D.J., The hydromagnetic stability of the magnetospheric boundary, Planet. Space Sci., 16, 587-605, 1968.

Spreiter, J.R. and A.Y. Alksne, Plasma flow around the magnetosphere, Rev. of Geophys., 7, 11-50, 1969.

Tsuda, T. Effective viscosity of a streaming collision-free plasma in a weakly turbulent magnetic field, J. Geophys. Res., 72, 6013-6020, 1967.

Warren, C.S. and J.W. Freeman, Jr., Evidence for viscous interaction at the magnetospheric boundary. Preprint from the Houston NASA Center 1970.

Captions

Fig. 1. Projection of the orbit of OGO 5 in the GSM equatorial plane at the time of the observations. The extreme extrapolated positions of the boundary are shown.

Fig. 2. Basic relations for tangential and rotational discontinuities. The projection of the magnetic field vectors on the two sides of the discontinuity, in the plane of this discontinuity are shown on the right.

Fig. 3. Variation of the magnetic field versus universal time on March 27, 1968. The GSM reference system is used; B_T refers to the total field.

Fig. 4. Variation of the magnetic field and particle flux versus time from 1719 to 1919 UT on March 27, 1968. The numbers from 1 to 6 refer to crossings which will be studied in Section 5. The particle flux unit is 10^4 particles/cm^2/sec/ster. See text for details.

Fig. 5. Schematic models of an equatorial section of the boundary.

Fig. 6. Projection on the X Y GSM plane of the tips of unitary vectors parallel to the largest eigenvectors ($\underline{x}$ in the text, open circles in the drawing)

and the smallest eigenvectors (z in the text, arrows in the drawing) for several crossings. z_1 and x_1 refer to the first crossing studied (see text). z and x refer to the unperturbed boundary. The circles indicate the locus of constant angle 30°, 45° and 90° with the Z GSM axis.

Fig. 7. Variation of the magnetic field through crossing as seen in the reference system xyz of the eigenvectors. The sampling rate is 56 sps.

Fig. 8. Evolution of the tip of the projection of the magnetic field in the plane xy of the boundary for crossing #1. Points are 1 sec apart.

Fig. 9 Variation of the magnetic field during spike #2 as shown in the reference system of the satellite. B_T is the total field. A zero base line is drawn for each component. A sampling rate of 56 sps is used.

Fig. 10. Shape of the boundary at the time of #2. The circled numbers are the values of B_x, computed from 1 sps data; the associated short arrows give the direction of the field projection in the zy plane. On the left, are shown various relevant directions as seen in the GSM equatorial plane (see text).

Fig. 11. Variation of the magnetic field through crossing b (Fig. 10) as seen in the reference system xyz of the eigenvectors.

Fig. 12. Variation of the magnetic field component in the eigenvector reference system xyz for interval n_{11} (crossing #3, Fig. A1). Points are 1 sec apart.

Fig. 13. Evolution of the tip of the projection of the magnetic field in the plane xy of the boundary for interval N_7 (crossing #3, Fig. A1). The points are 1.7×10^{-2} sec apart (56 sps). The dashed lines are drawn to emphasize the regions where $\underline{\nabla}B$ is parallel to $\underline{B}$. The average value of B_z ($3.5\ 10^{-2}\gamma$) for the interval AB is less than the digitization error of the instrument and so is equivalent to zero.

Fig. 14. Variation of the magnetic field components in the eigenvector reference system for interval n_8 (crossing #4, Fig. A2). Points are 1 sec apart.

Fig. 15. Evolution of the tip of the projection of the magnetic field in the plane xy of the boundary for interval N_6 (crossing #4, Fig. A2). The points are 1.7×10^{-2} sec apart (56 sps).

Fig. 16. Sketch of the boundary at the time of the crossings #3 and #4. Not to scale.

Fig. 17. Variation of the magnetic field through the spike #6 (Fig. 4). The satellite reference system 1, 2, 3 is used, as in Fig. 9. A zero base line is drawn for each component. A sampling rate of 56 sps is used.

Fig. A1. Variation of the B_1 component (reference system of the satellite) versus time, through crossing #3. The sampling rate is 56 sps. The intervals labelled N_1 to n_{11} were used for eigenvalue computations. The resulting directions of the largest (open circles) and smallest (arrows) eigenvectors are represented at the top left of the figure (same system of representation as in Fig. 6). x and z refer to the unperturbed boundary.

Fig. A2. Variations of the B_1 component (reference system of the satellite) versus time through crossing #4. The sampling rate is 56 sps. The intervals labelled N_1 to n_{10} were used for eigenvalue computations. The resulting directions of the largest (open circles) and smallest (arrows) eigenvectors are represented at the top right of the figure (same system of representation as in Fig. 6). x and z refer to the unperturbed boundary.

Table 1. Results of the eigenvalue computation for several time intervals during the crossing #3.

Table 2. Results of the eigenvalue computation for several time intervals during the crossing #4.

Table 1

Interval	Number of Samples	$\overline{B_z}(\gamma)$	σ^2	Eigenvalue Ratios: Maximum / Intermediate	Eigenvalue Ratios: Intermediate / Minimum
N_1	625	+2.6	7.2	18.8	5.9
N_2	73	-10.2	0.1	9.1	24.7
N_3	36	-6.1	0.03	56.9	17.1
N_4	58	-22.4	0.1	6.8	2.9
N_5	51	-10.0	0.04	12.9	5.7
N_6	51	+7.3	0.2	6.5	4.0
N_7	100	-0.5	1.5	6.3	33.6
N_8	50	-0.7	2.0	7.3	16.7
N_9	50	+0.4	0.3	5.4	8.8
n_{10}	8	+10.3	7.7	31.6	2.8
n_{11}	11	+4.7	5.9	29.7	4.4

Table 2

Interval	Number of Samples	$\overline{B_z(\gamma)}$	σ^2	Eigenvalue Ratios: Maximum / Intermediate	Eigenvalue Ratios: Intermediate / Minimum
N_1	109	13.6	0.1	11.2	198.4
N_2	45	4.4	0.1	5.1	19.1
N_3	67	9.2	0.8	12.8	11.4
N_4	221	11.1	1.9	7.3	43.4
N_5	36	10.8	0.03	135.2	13.5
N_6	59	12.4	0.1	38.8	21.8
N_7	669	8.8	3.7	23.4	15.3
n_8	12	13.2	6.0	90.8	2.3
n_9	14	12.2	9.7	104.7	1.3
n_{10}	7	14.5	4.3	56.7	3.9

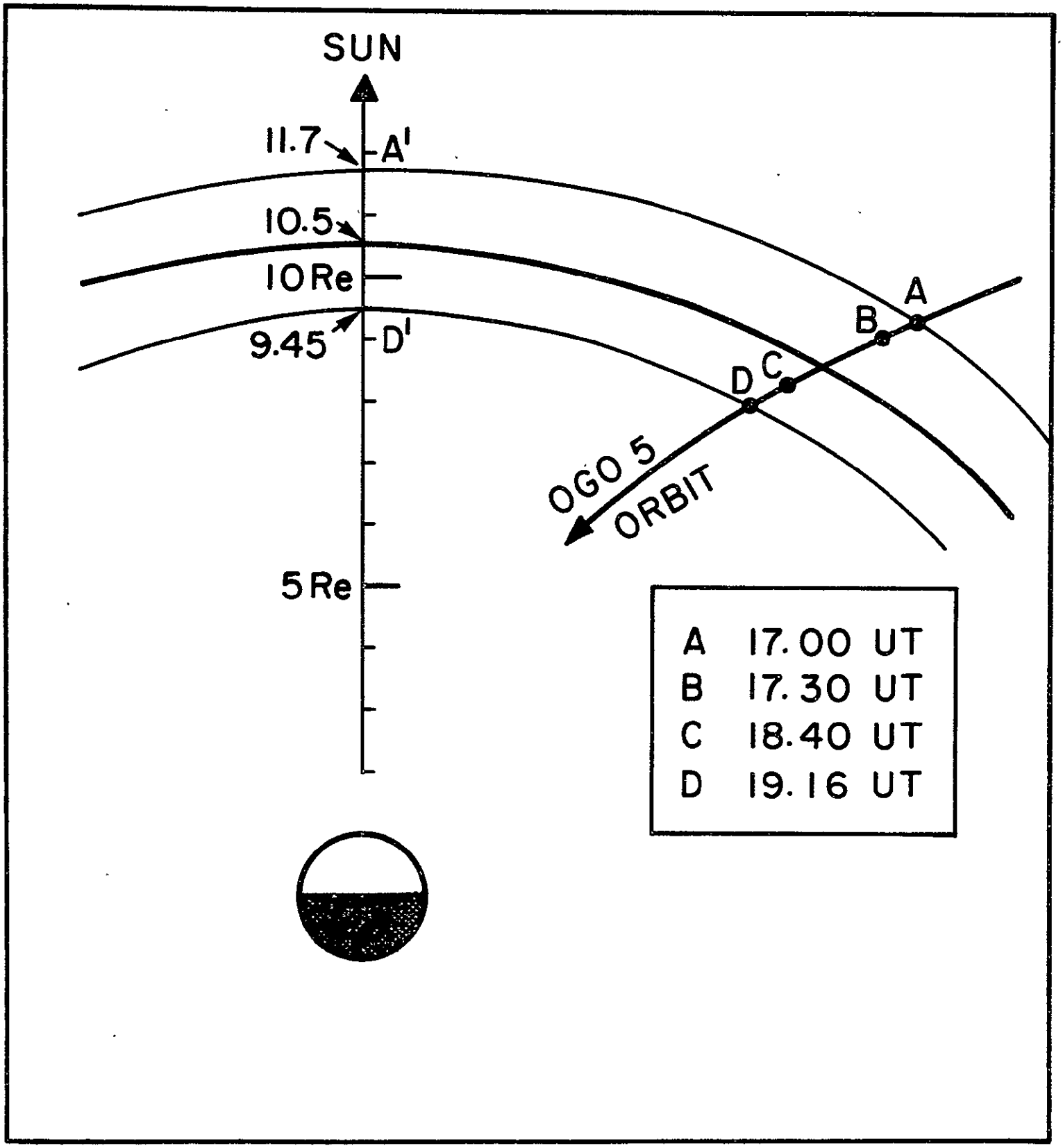
SUN
11.7
A'
10.5
10 Re
9.45
D'
5 Re
A
B
C
D
OGO 5
ORBIT
A 17.00 UT
B 17.30 UT
C 18.40 UT
D 19.16 UT

Fig. 1

TANGENTIAL DISCONTINUITY

$$\rho v_n = 0 \quad , \quad [\vec{v}_t] \neq 0 \quad , \quad [\rho] \neq 0 \ ,$$

$$\left[p + \frac{H_t^2}{8\pi}\right] = 0 \quad , \quad H_n = 0 \quad , [\vec{H}_t] \neq 0 \ ,$$

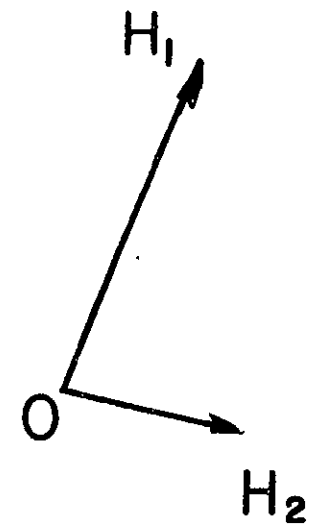

ROTATIONAL DISCONTINUITY

$$\rho v_n \neq 0 \quad , \quad [\vec{v}_t] \neq 0 \quad , \quad [\rho] = 0 \ ,$$

$$[p] = 0 \quad , \quad H_n \neq 0 \ , \quad [\vec{v}_t] = \frac{[\vec{H}_t]}{\sqrt{4\pi\rho}} \ ,$$

$$[|H|] = 0$$

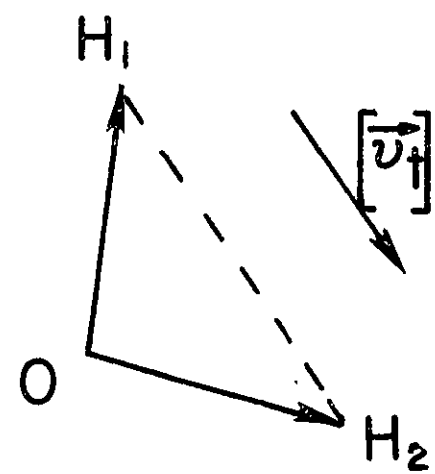

Fig. 2

UCLA OGO-5 FLUXGATE MAGNETOMETER
GSM COORDINATES

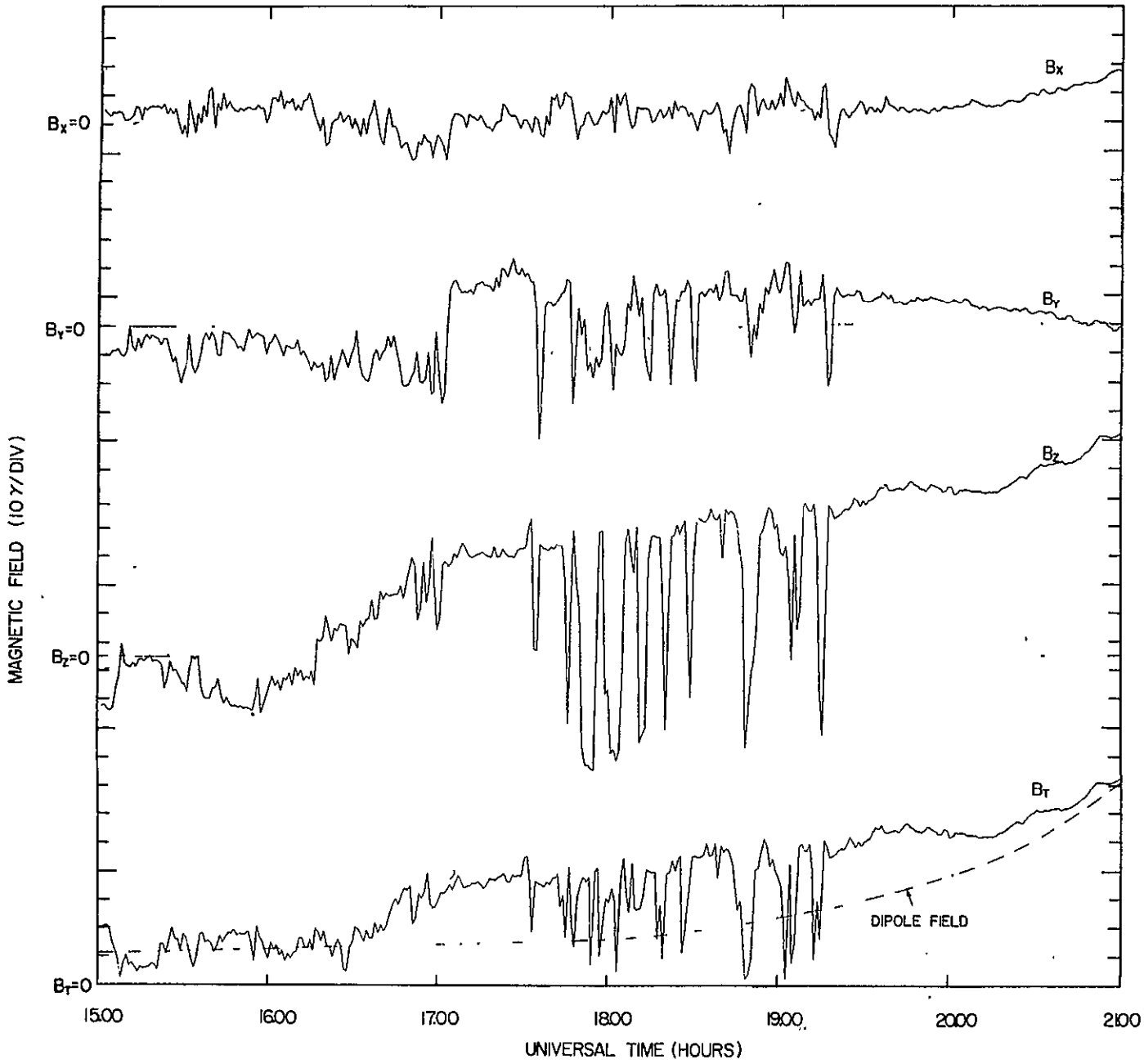

Fig. 3

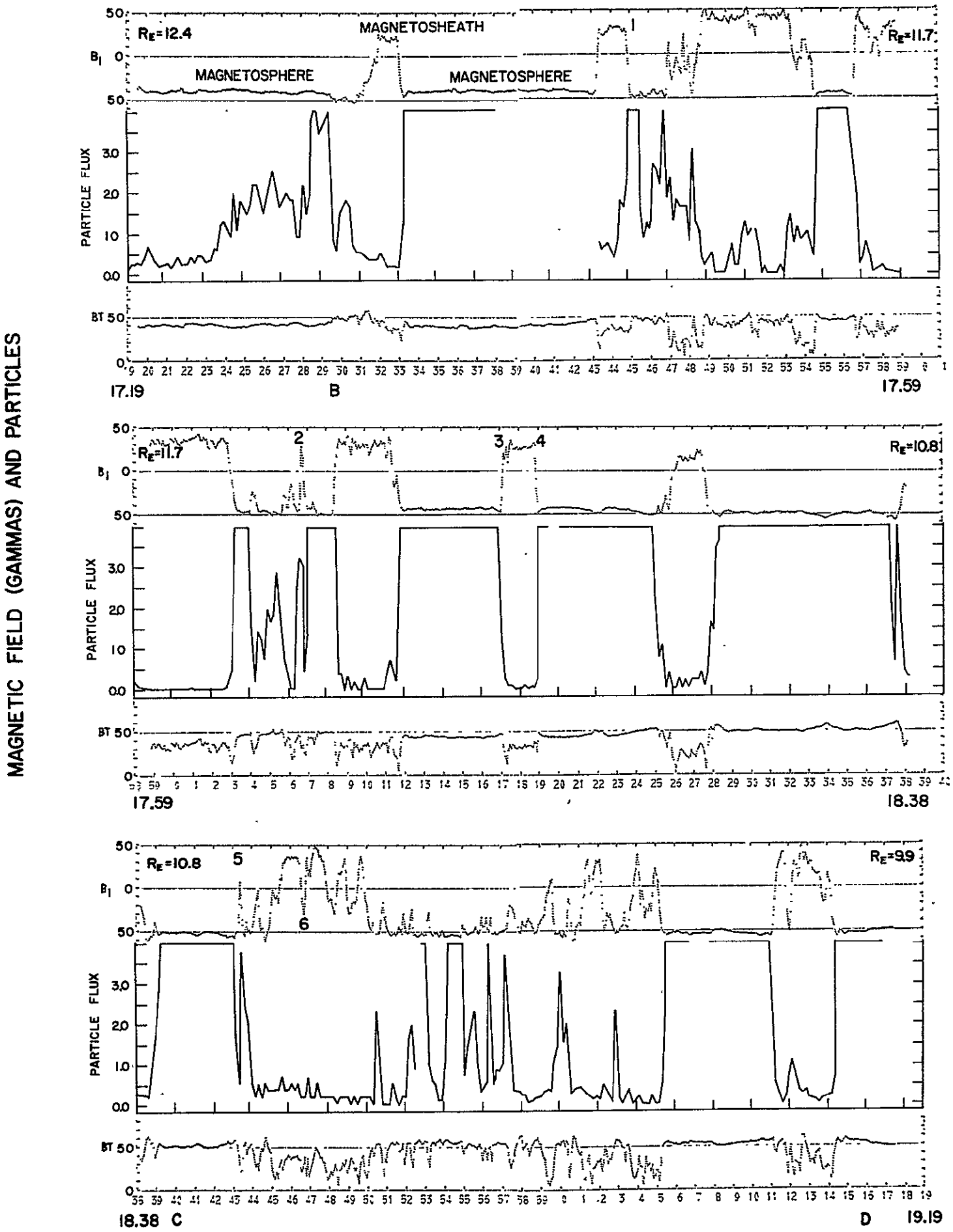
MAGNETIC FIELD (GAMMAS) AND PARTICLES
R_E=12.4
MAGNETOSHEATH
MAGNETOSPHERE
MAGNETOSPHERE
R_E=11.7
B_I
PARTICLE FLUX
BT
17.19
B
17.59
R_E=11.7
R_E=10.8
17.59
18.38
R_E=10.8
R_E=9.9
18.38 C
D 19.19
UNIVERSAL TIME

Fig. 4

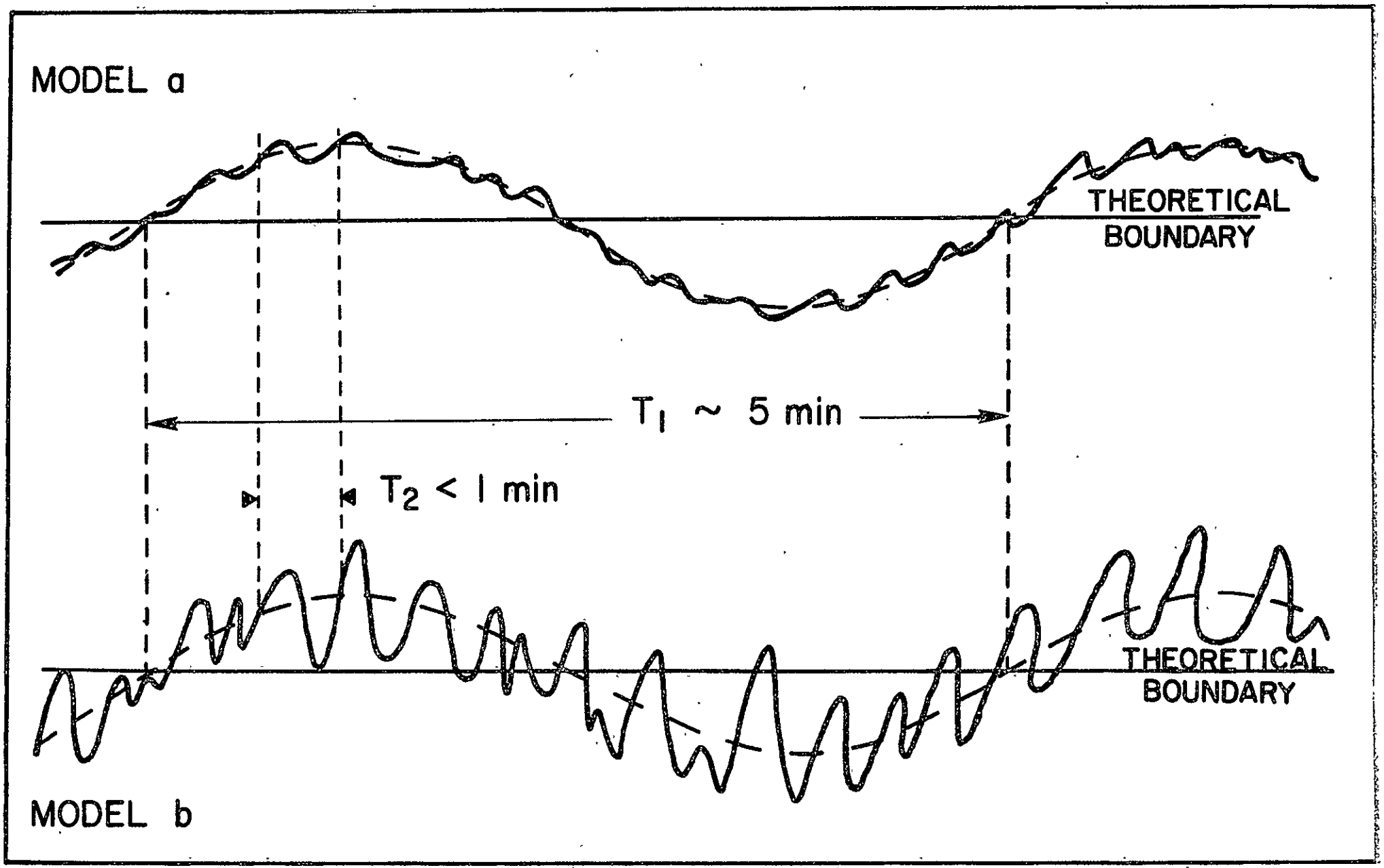
MODEL a
THEORETICAL BOUNDARY
$T_1 \sim 5$ min
$T_2 < 1$ min
THEORETICAL BOUNDARY
MODEL b

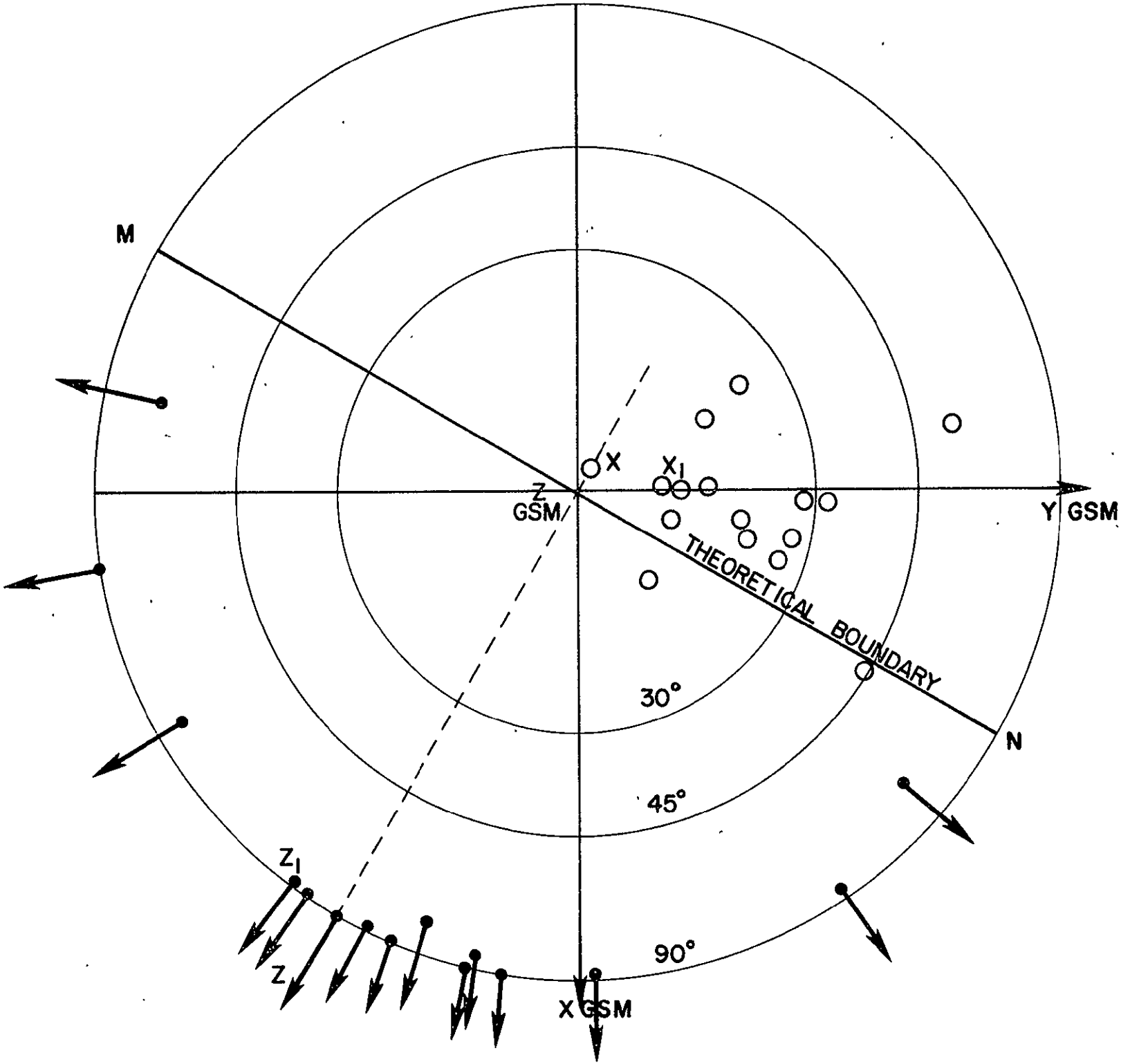

Fig. 6

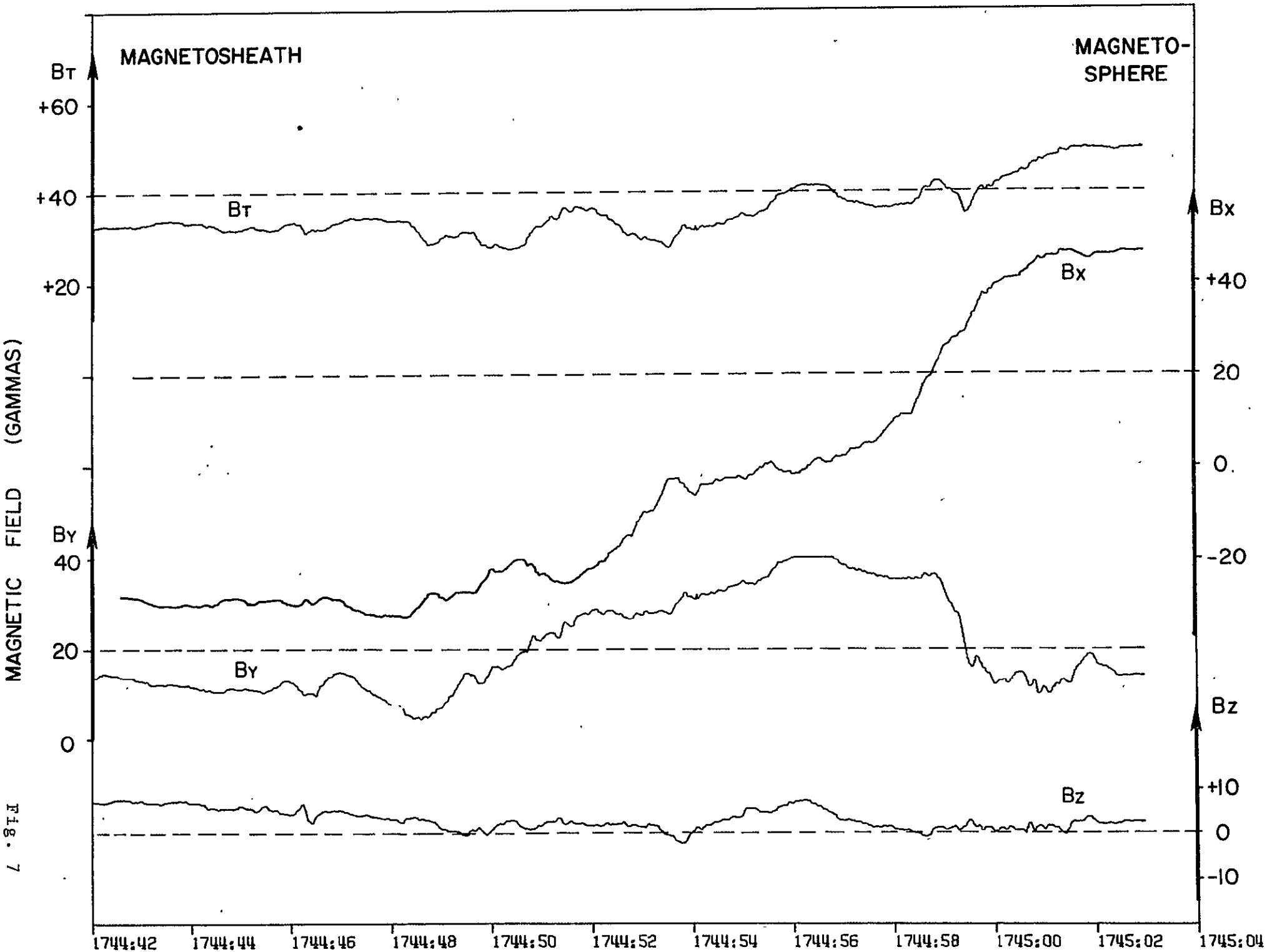
MAGNETOSHEATH
MAGNETO-
SPHERE
MAGNETIC FIELD (GAMMAS)
BT
+60
+40
+20
BT
BY
40
20
0
BY
Bx
+40
20
0
-20
Bx
Bz
+10
0
-10
Bz
1744:42
1744:44
1744:46
1744:48
1744:50
1744:52
1744:54
1744:56
1744:58
1745:00
1745:02
1745:04

Fig. 7

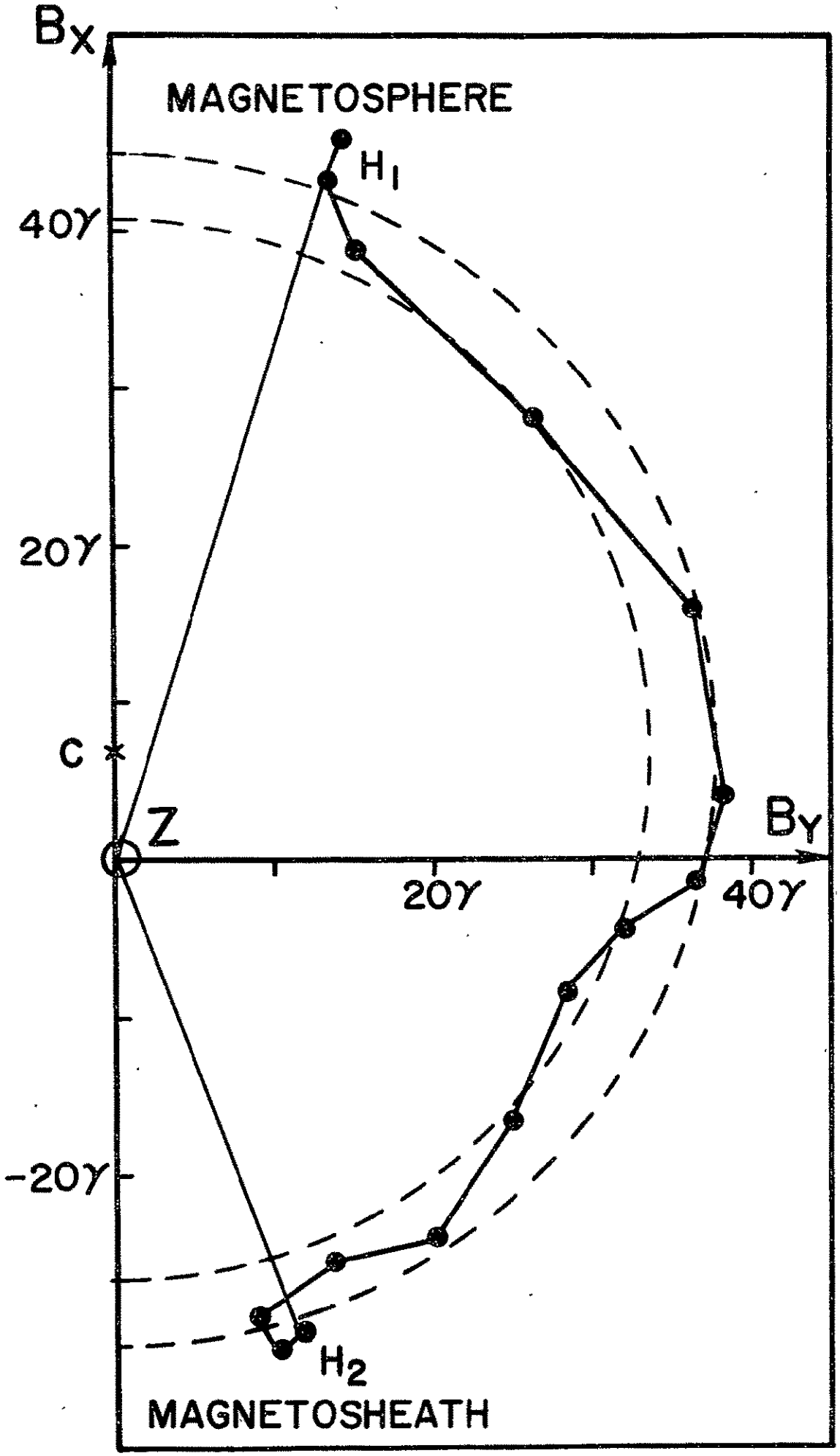
Bx
MAGNETOSPHERE
H1
40γ
20γ
C
Z
By
20γ
40γ
-20γ
H2
MAGNETOSHEATH

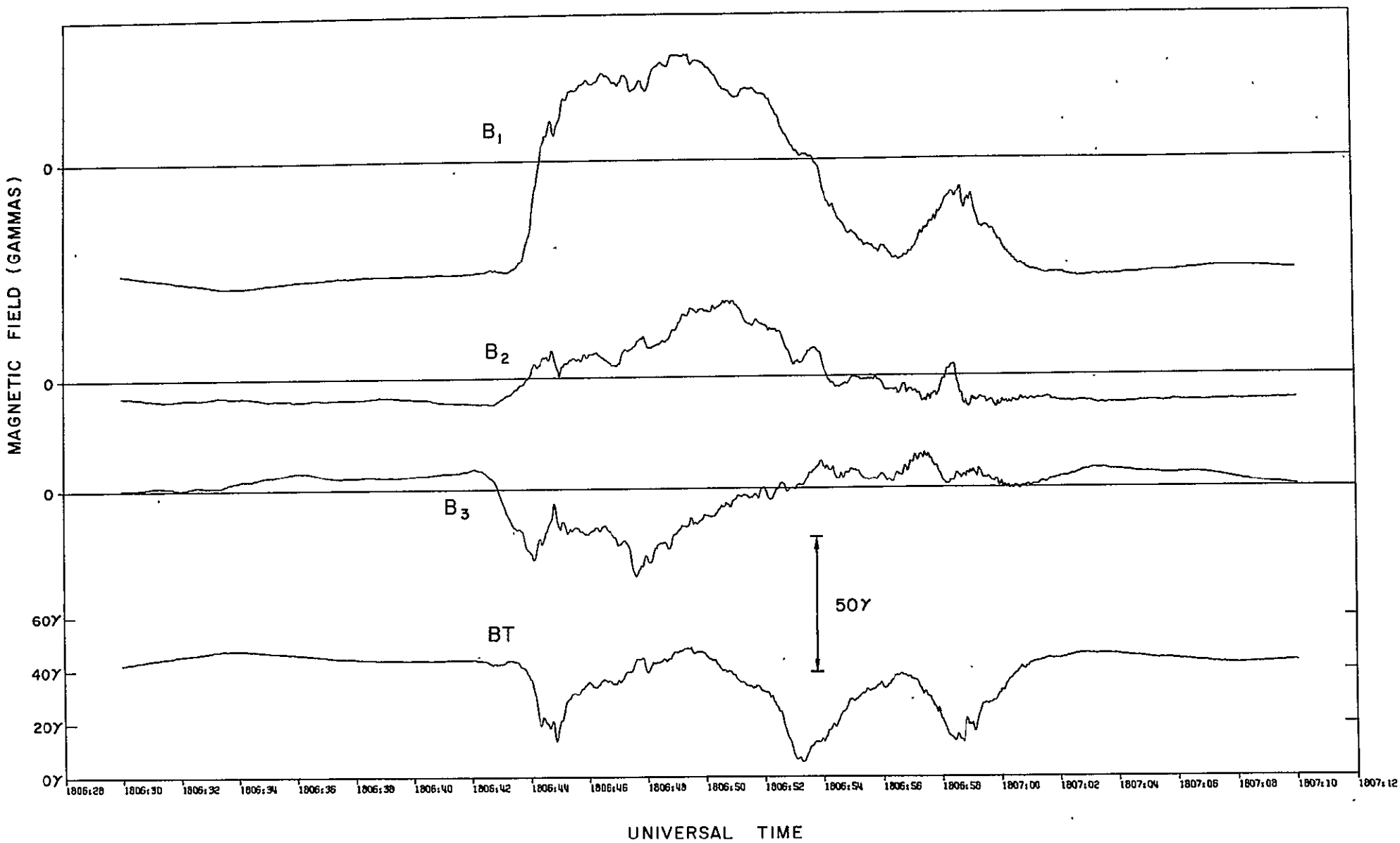
MAGNETIC FIELD (GAMMAS)
0
0
0
60γ
40γ
20γ
0γ
B1
B2
B3
BT
50γ
1806:28
1806:30
1806:32
1806:34
1806:36
1806:38
1806:40
1806:42
1806:44
1806:46
1806:48
1806:50
1806:52
1806:54
1806:56
1806:58
1807:00
1807:02
1807:04
1807:06
1807:08
1807:10
1807:12
UNIVERSAL TIME

Fig. 9

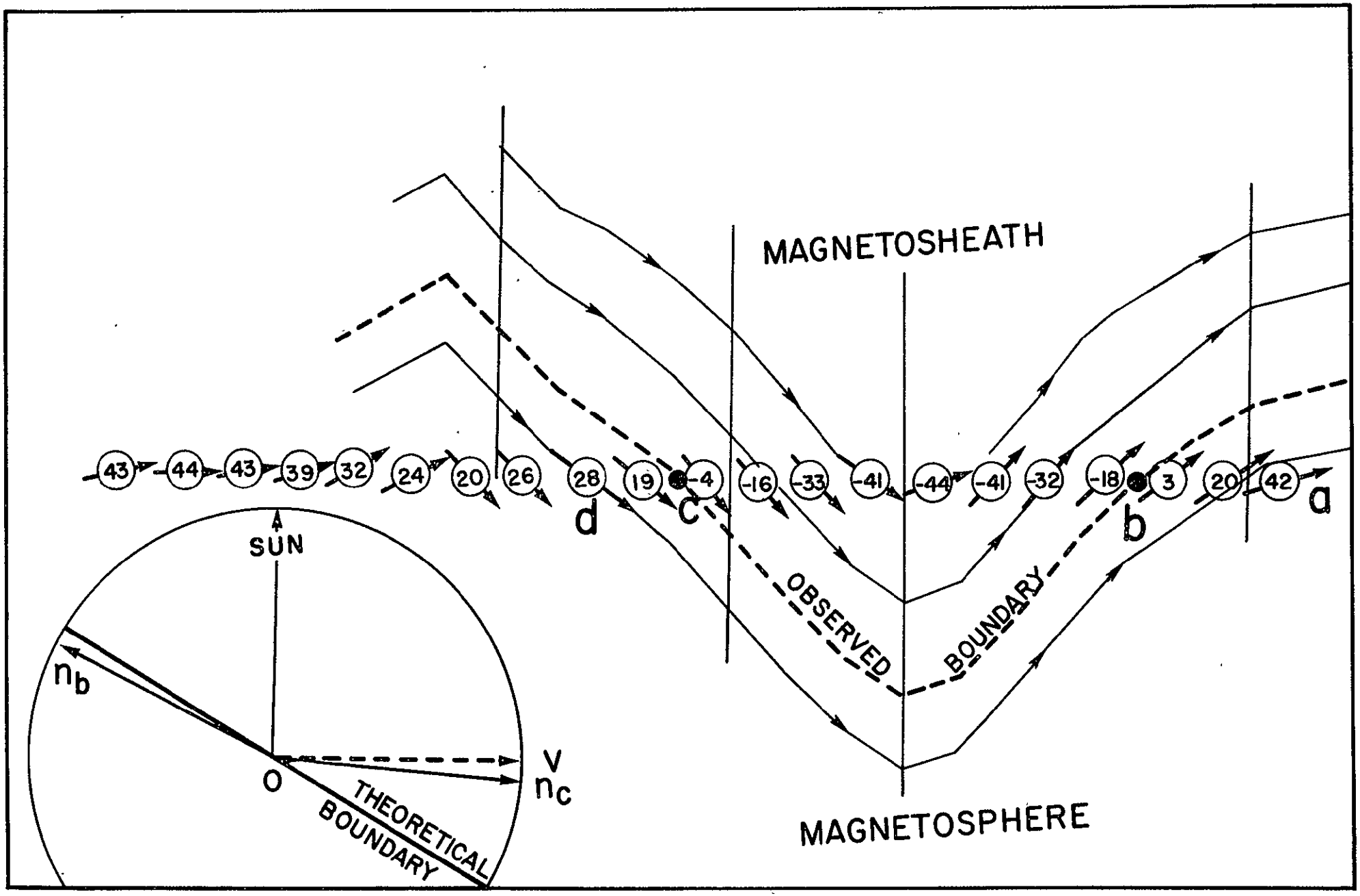
MAGNETOSHEATH
MAGNETOSPHERE
OBSERVED BOUNDARY
THEORETICAL BOUNDARY
SUN
O
n_b
n_c
V
43
44
43
39
32
24
20
26
28
19
-4
-16
-33
-41
-44
-41
-32
-18
3
20
42
a
b
c
d

Fig. 10

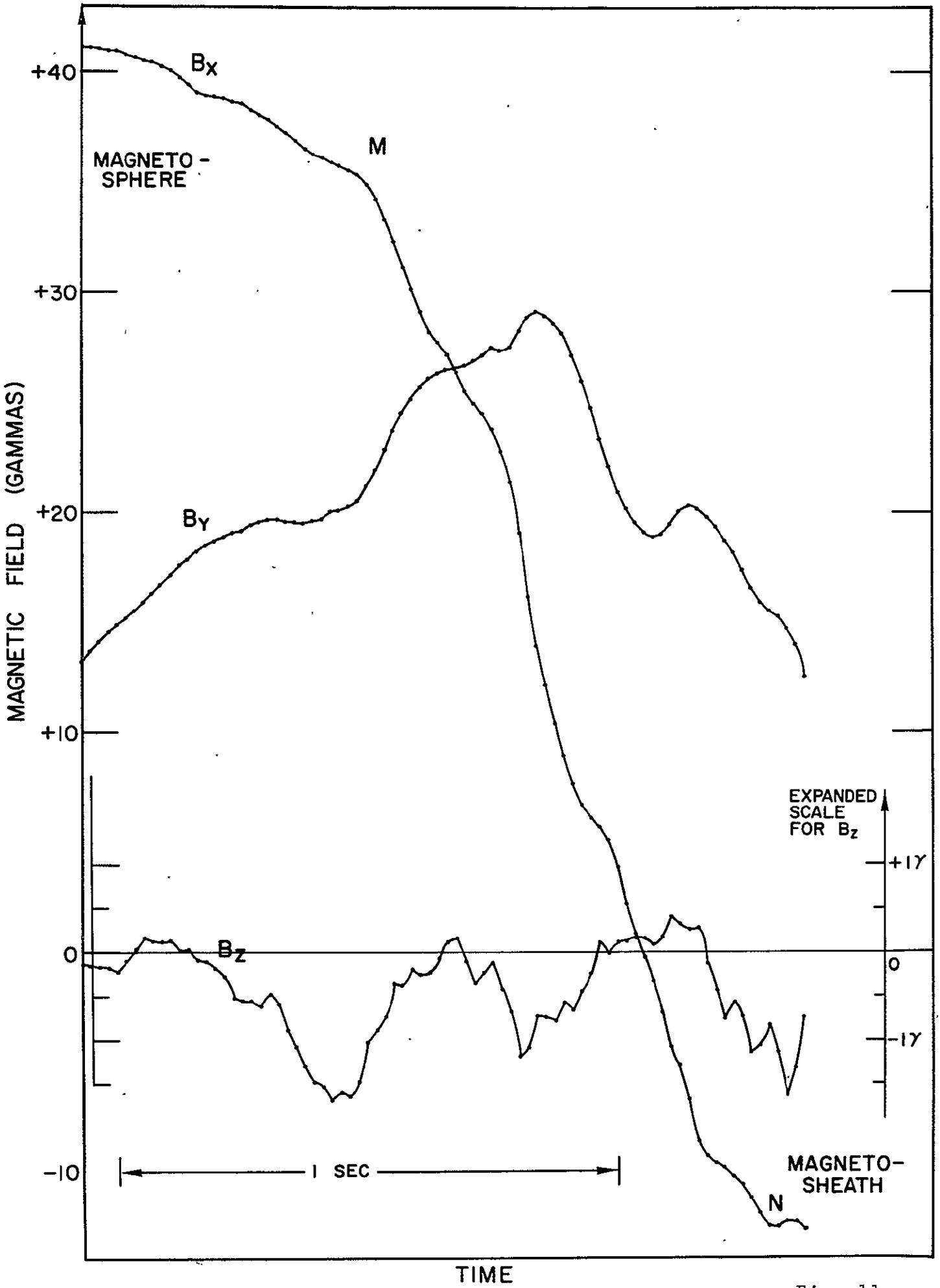
+40
+30
+20
+10
0
-10
MAGNETIC FIELD (GAMMAS)
Bx
By
Bz
M
N
MAGNETO-
SPHERE
MAGNETO-
SHEATH
EXPANDED
SCALE
FOR Bz
+1γ
0
-1γ
1 SEC
TIME

Fig. 11

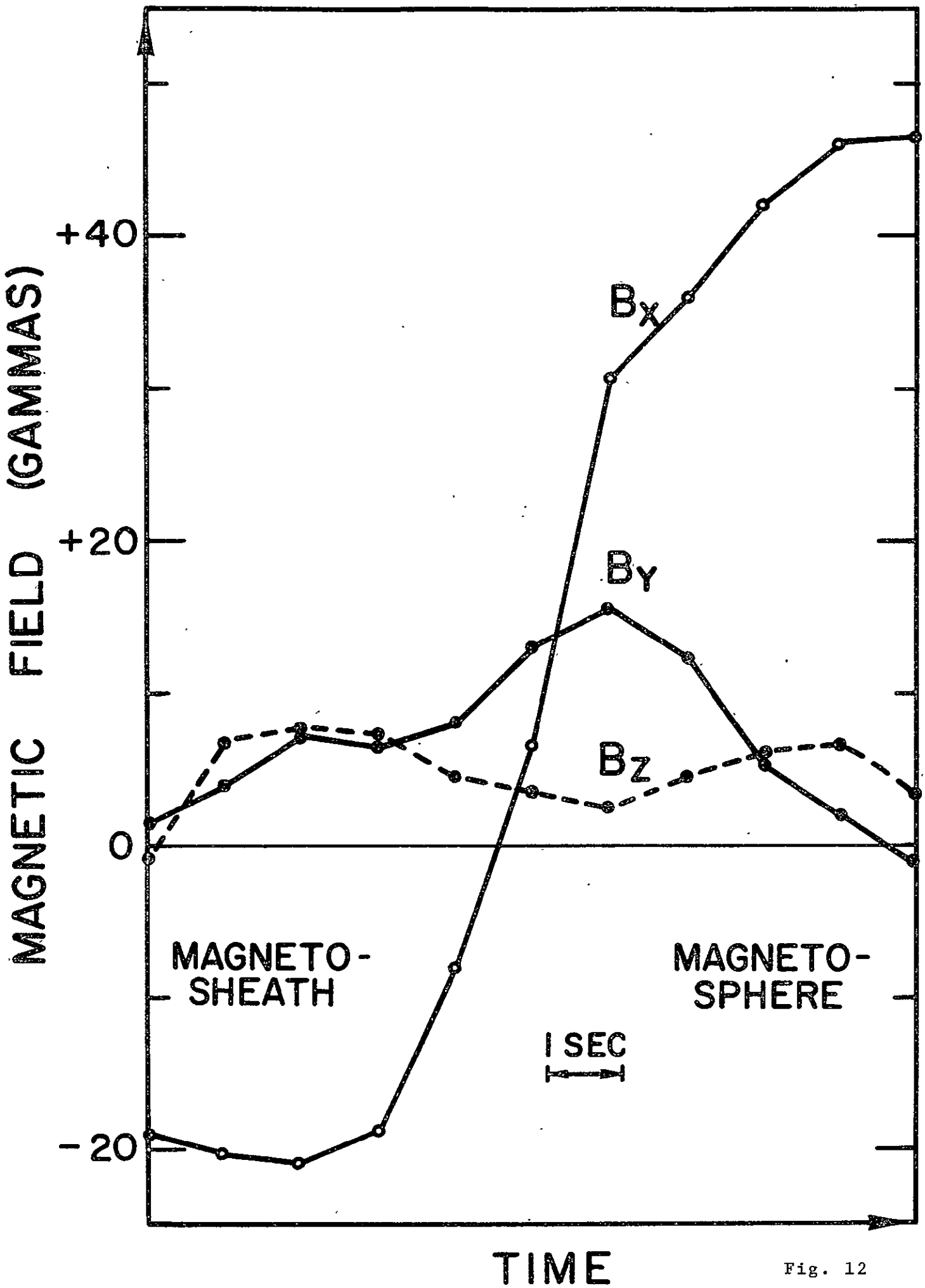
MAGNETIC FIELD (GAMMAS)
+40
+20
0
-20
B_X
B_Y
B_Z
MAGNETO-
SHEATH
MAGNETO-
SPHERE
1 SEC
TIME

Fig. 12

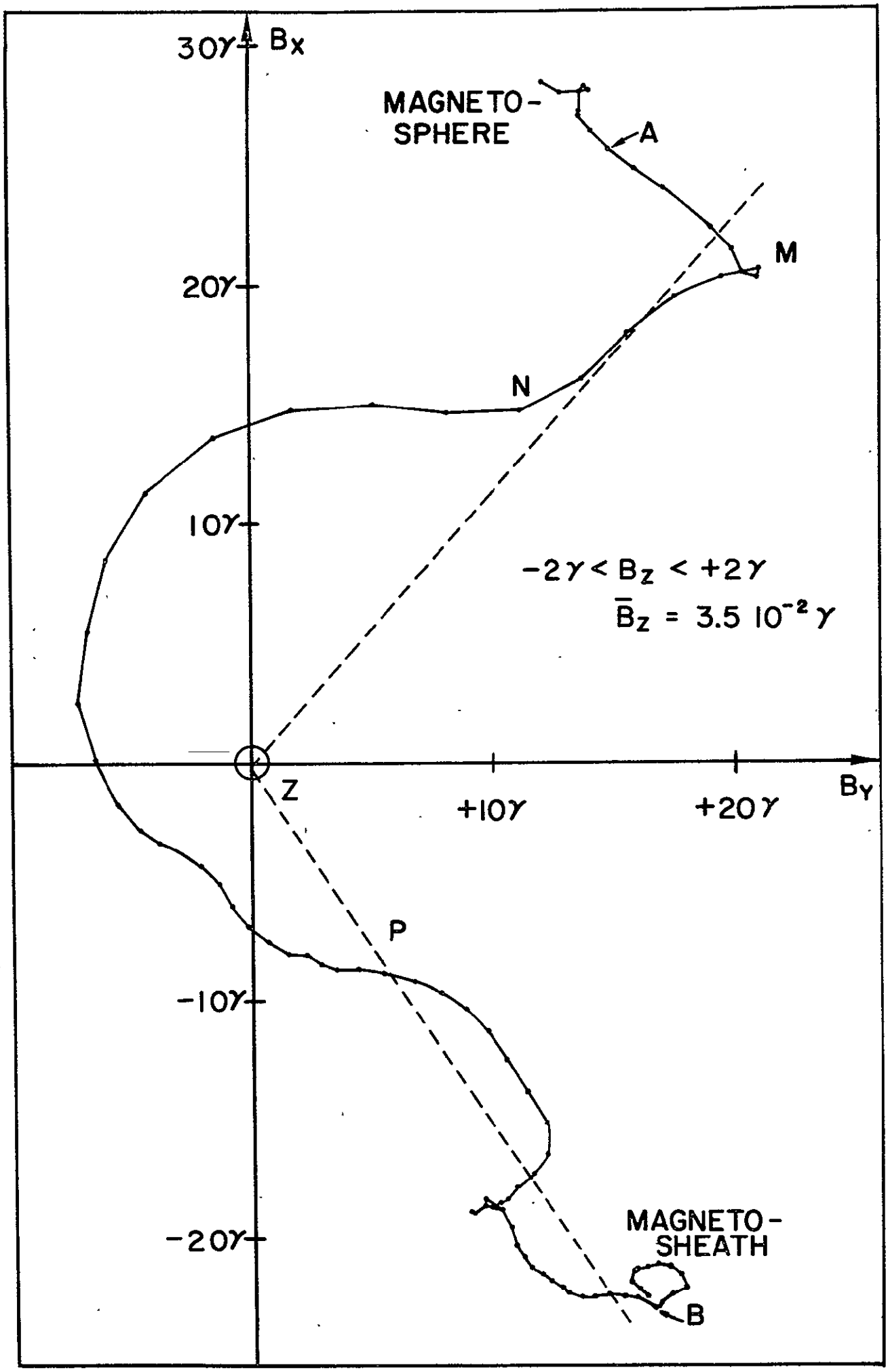
30γ
Bx
MAGNETO-
SPHERE
A
M
20γ
N
10γ
−2γ < Bz < +2γ
B̄z = 3.5 10⁻² γ
Z
+10γ
+20γ
BY
P
−10γ
−20γ
MAGNETO-
SHEATH
B

Fig. 13

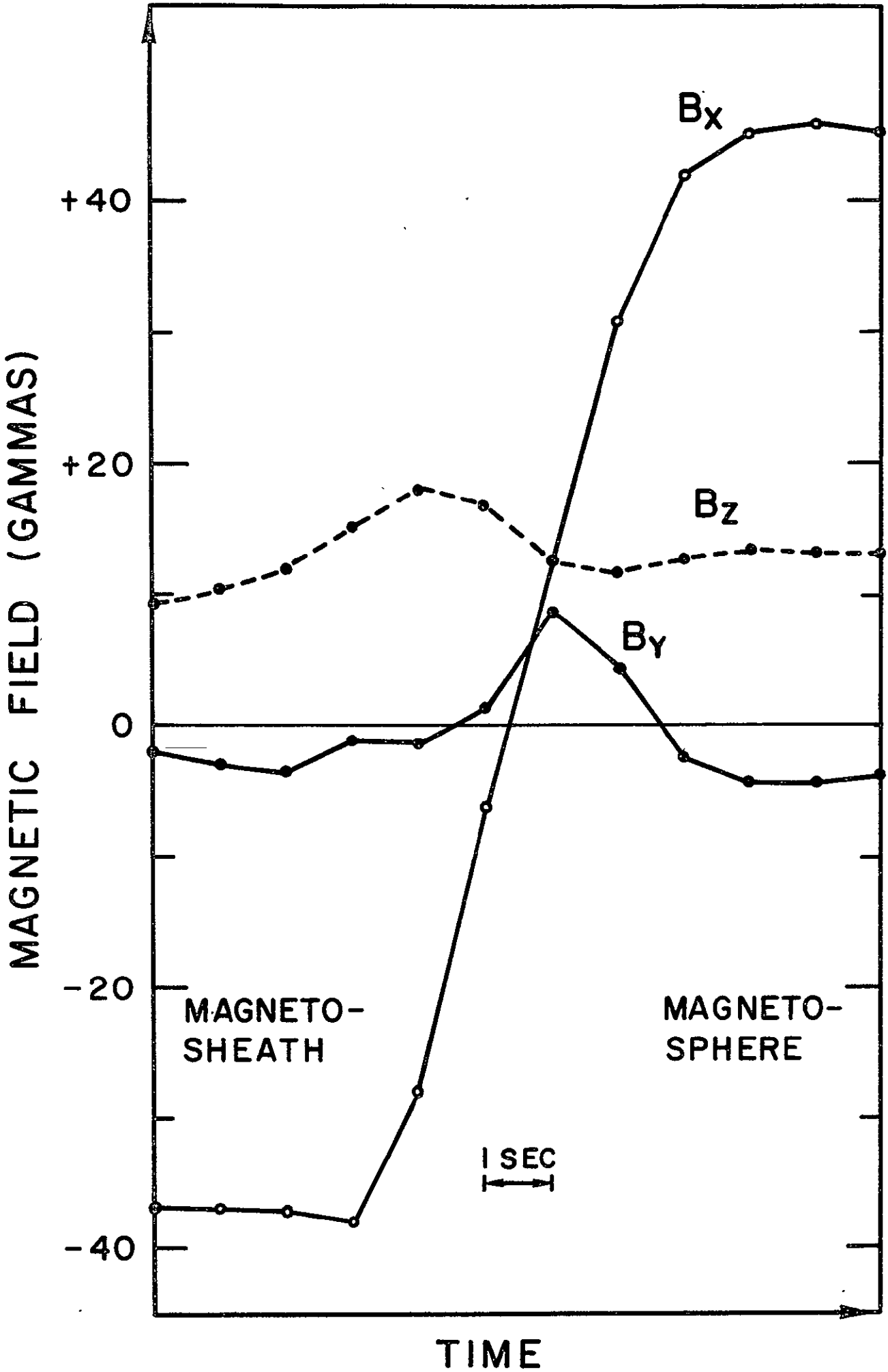
MAGNETIC FIELD (GAMMAS)
+40
+20
0
-20
-40
B_X
B_Z
B_Y
MAGNETO-
SHEATH
MAGNETO-
SPHERE
1 SEC
TIME

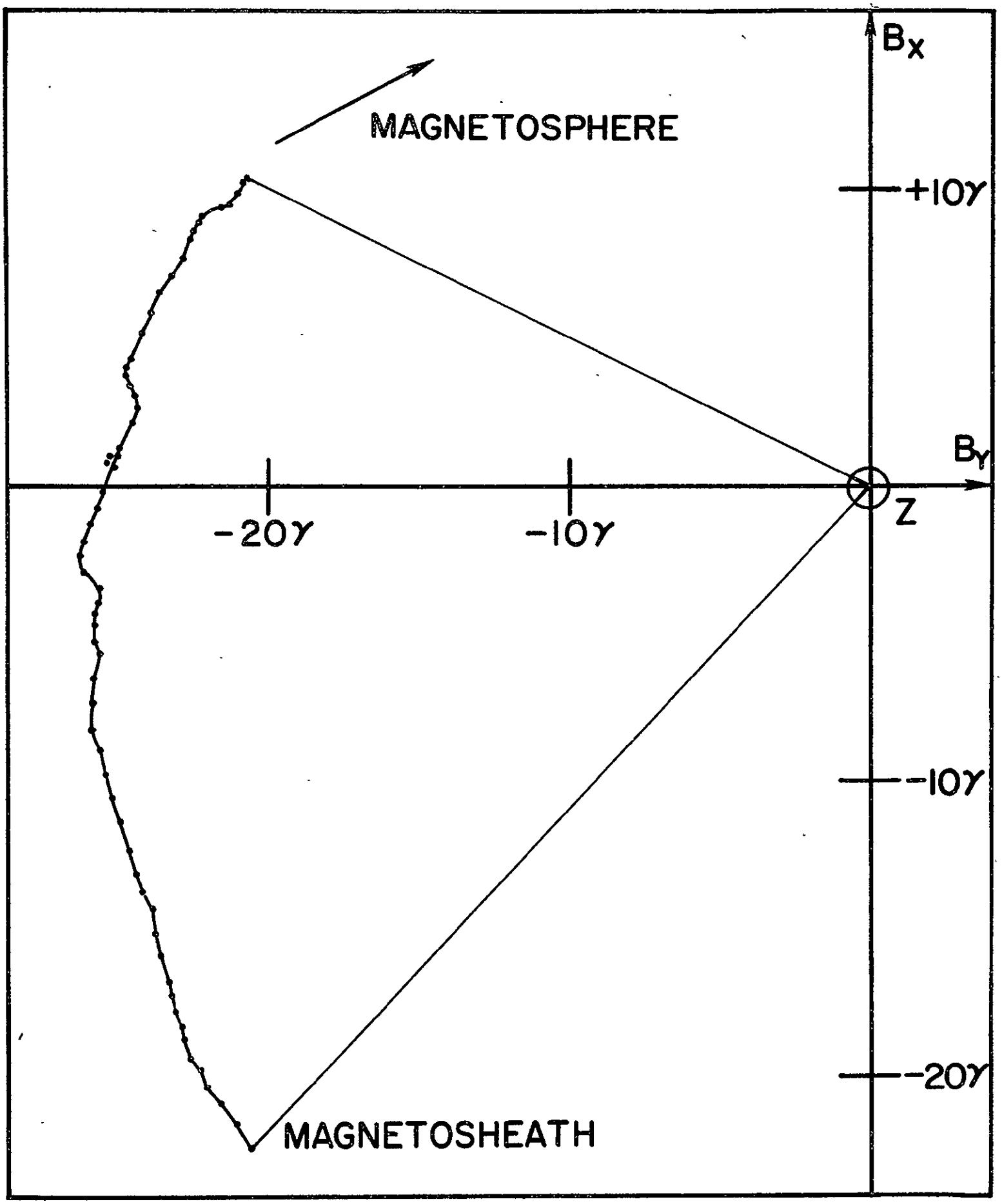
B_X
MAGNETOSPHERE
+10γ
B_Y
Z
-20γ
-10γ
-10γ
-20γ
MAGNETOSHEATH

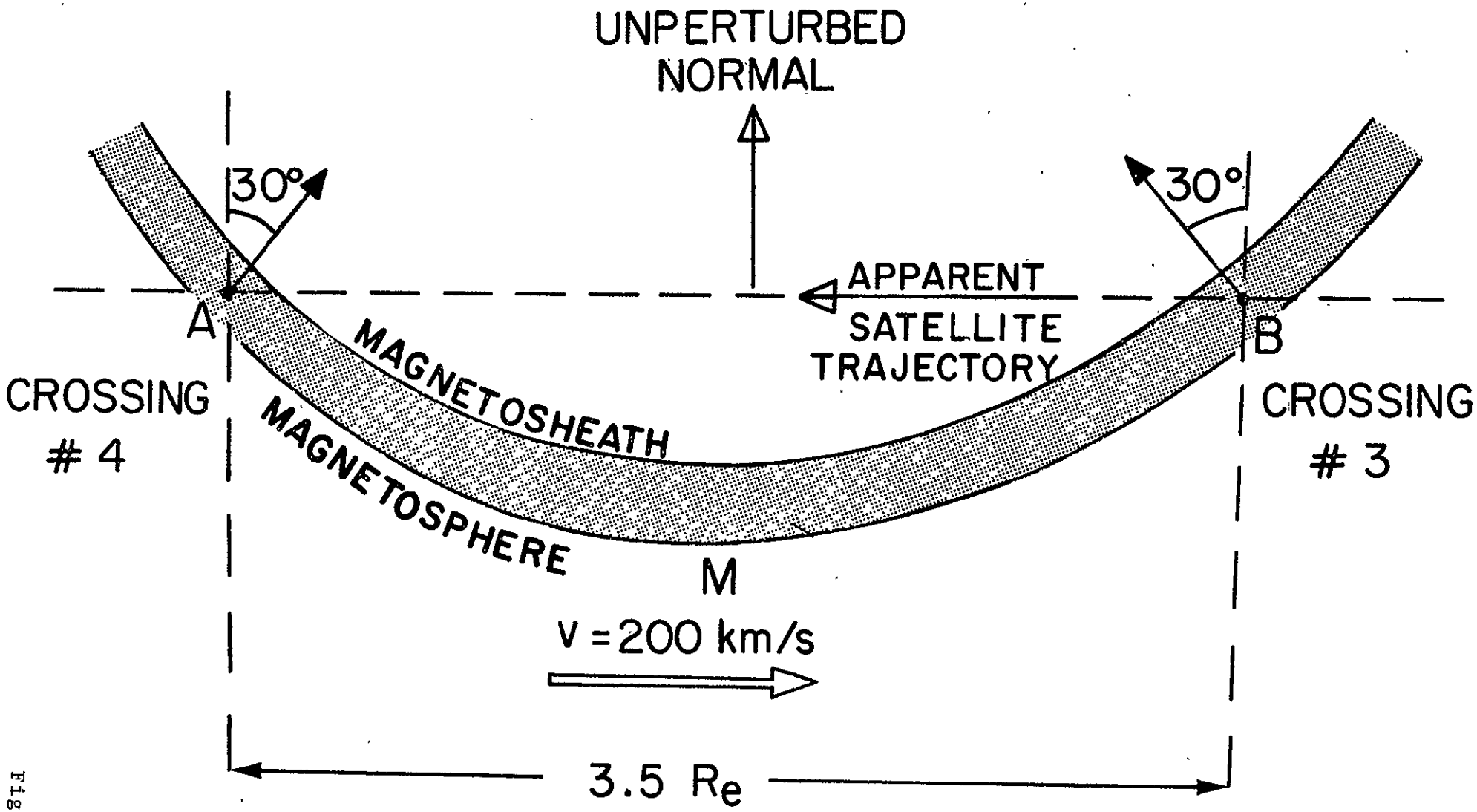
UNPERTURBED
NORMAL
30°
30°
APPARENT
SATELLITE
TRAJECTORY
A
B
CROSSING
4
CROSSING
3
MAGNETOSHEATH
MAGNETOSPHERE
M
V = 200 km/s
3.5 Re

Fig. 16

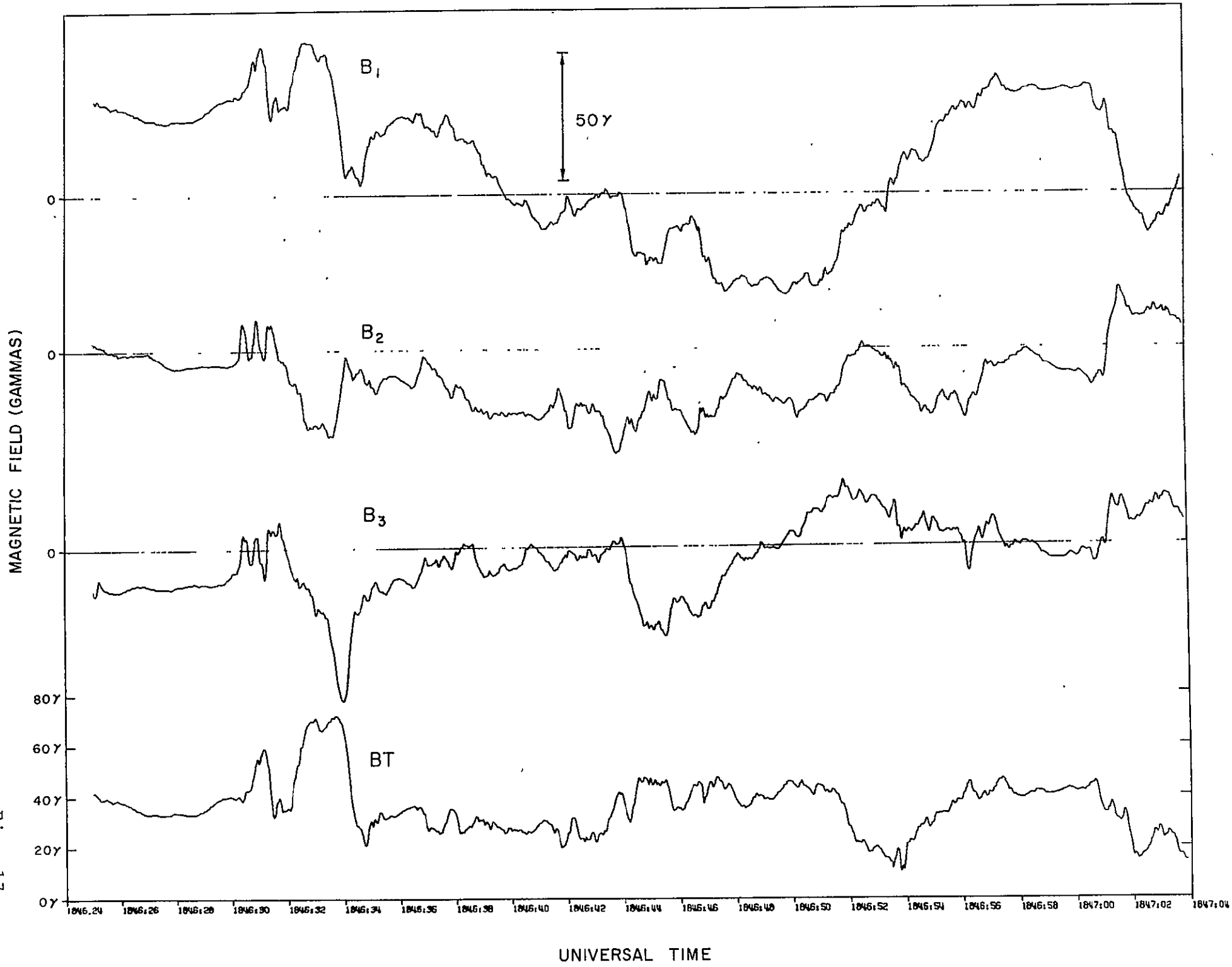
B1
50γ
0
B2
0
B3
0
80γ
60γ
40γ
20γ
0γ
BT
MAGNETIC FIELD (GAMMAS)
1846:24
1846:26
1846:28
1846:30
1846:32
1846:34
1846:36
1846:38
1846:40
1846:42
1846:44
1846:46
1846:48
1846:50
1846:52
1846:54
1846:56
1846:58
1847:00
1847:02
1847:04
UNIVERSAL TIME

Fig. 17

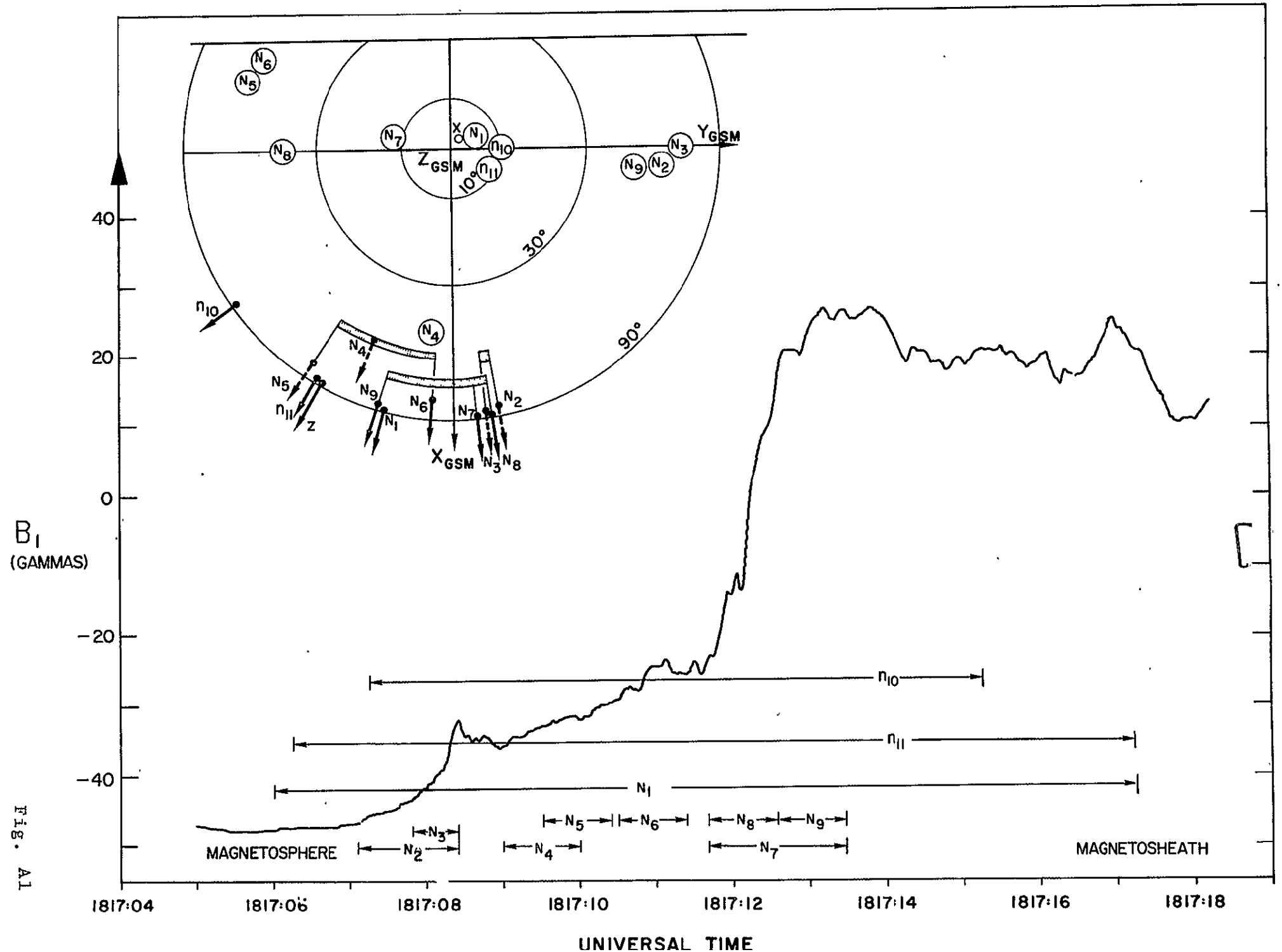
B_1
(GAMMAS)
40
20
0
-20
-40
1817:04
1817:06
1817:08
1817:10
1817:12
1817:14
1817:16
1817:18
UNIVERSAL TIME
MAGNETOSPHERE
MAGNETOSHEATH
n_{10}
n_{11}
N_1
N_2
N_3
N_4
N_5
N_6
N_7
N_8
N_9
Y_{GSM}
Z_{GSM}
X_{GSM}
X
Z
10°
30°
90°

Fig. A1

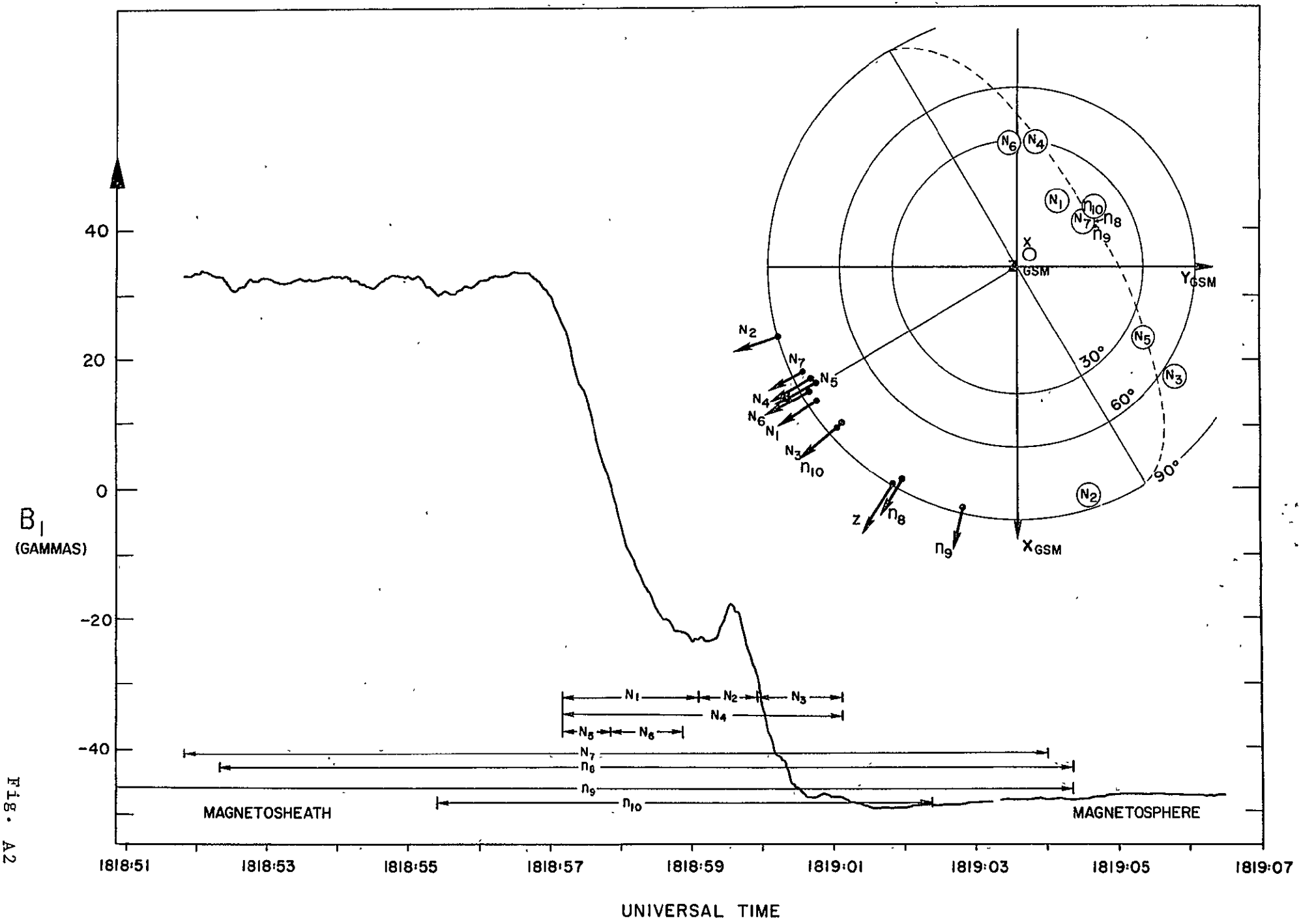
40
20
0
-20
-40
B_1
(GAMMAS)
1818:51
1818:53
1818:55
1818:57
1818:59
1819:01
1819:03
1819:05
1819:07
UNIVERSAL TIME
MAGNETOSHEATH
MAGNETOSPHERE
N_1
N_2
N_3
N_4
N_5
N_6
N_7
n_6
n_9
n_{10}
X_{GSM}
Y_{GSM}
Z
30°
60°
90°
n_8

Fig. A2